IEEE Access
Multidisciplinary | Rapid Review | Open Access Journal

Received 19 April 2024, accepted 8 May 2024, date of publication 13 May 2024, date of current version 20 June 2024.

Digital Object Identifier 10.1109/ACCESS.2024.3400038

RESEARCH ARTICLE

Accurate Identification of Harmonic Distortion for Micro-Grids Using Artificial Intelligence-Based Predictive Models

AHMED M. ABED[1,2], RAGAB A. EL-SEHIEMY[3], (Senior Member, IEEE), BACHIR BENTOUATI[4], AND HASNAA M. EL-ARWASH[5]

[1]Department of Industrial Engineering, College of Engineering, Prince Sattam bin Abdulaziz University, Al-Kharj 16273, Saudi Arabia
[2]Industrial Engineering Department, Zagazig University, Zagazig 44519, Egypt
[3]Electrical Engineering Department, Faculty of Engineering, Kafrelsheikh University, Kafr El-Sheikh 6860404, Egypt
[4]Department of Electrical Engineering, Université Amar Telidji Laghouat, Laghouat 03000, Algeria
[5]Department of Mechatronics Engineering, Alexandria Higher Institute of Engineering and Technology (AIET), Alexandria 21311, Egypt

Corresponding authors: Ahmed M. Abed (A.abed@psau.edu.sa) and Hasnaa M. El-Arwash (hasnaa.mohamed@aiet.edu.eg)

This work was supported in part by Prince Sattam bin Abdulaziz University (PSAU) as part of funding for its Sustainable Development Goals (SDG) Roadmap Research Funding Program under Project PSAU-2023-SDG-22.

ABSTRACT This paper proposes an accurate harmonic identification strategy for microgrids and distributed power systems. The harmonic identification strategy is one of the complex tasks in microgrids due to the need of high computational burden in terms of memory and computational time. The complexity of the considered problem is resulted from solving the transcendental nonlinear equations that characterize harmonics especially in real time is considered as a highly challenged problem. The proposed identification strategy aims at detecting individual and total harmonic distortion levels that is generated from several harmonic sources. In the current paper, the Machine Learning Regression Analysis (MLRA) including location-specific data and the Artificial Neural Networks (ANNs) are proposed to identify the harmonic distortion. To enhance the identification and prediction performance, the standard IEEE 34-bus test feeder with verified harmonic sources power system is emulated for various scenarios using Electric Transient Analysis Program (ETAP). An extracting procedure for individual and total harmonic components are employed. The higher reduction level of error with approximately maximum median of $3.7127e{-}15\%$ assures the accurate prediction of harmonic components. In addition, this work investigates the impact of several practical cases when the voltages of the renewable clean energy source arrays vary (e.g., solar cell, wind turbine, and EV), and a double-stage topology is needed to have the same amount of voltage at the input of the inverter before inversion.

INDEX TERMS ANNs, ETAP, harmonic distortion, machine learning, micro-grid.

PREAMBLE

Our research aims to improve the quality of energy in micro-grids, which achieve abundance in electricity, to meet the SDG 8 target, which promotes inclusive, and sustainable economic growth and productivity. We want to ensure the well-being of citizens when they find decent work, raise their satisfaction level (CSL), which is tracked via welfare and satisfaction growth indicator (WSGI) and the GDP/capita. This will also help to develop investment in the energy sector.

The associate editor coordinating the review of this manuscript and approving it for publication was Dinesh Kumar.

I. INTRODUCTION

Growing energy consumption and policies aimed at reducing greenhouse gas emissions. Reduction of the gas emission is considered as the primary driver of the global trend towards the use of greener energy systems in the power field. A micro-grid is a small collection of electrical loads and sources that are typically linked together and acts as a part of the larger conventional central electrical grid. The microgrid functions are independently based on the demands of the external environment and/or the economy It allows for the effective integration of various clean power sources, integrating greener technologies like electric vehicles (EVs), wind

turbines (WTs), and solar photovoltaics (PVs) into today's power grids is one potential solution [1].

The increasing worries about the quality of electricity in modern electrical systems that have significant Renewable Energy Sources (RES) penetration are seriously threatened by harmonics and waveform distortion. In the past few decades, this topic has received increased attention due to the continuous and high percentage of adding power electronic devices that emulate nonlinear loads. Several tasks such as harmonic data clustering, filter-based harmonic elimination, harmonic data classification, harmonic source contribution estimation, waveform estimation, or prediction are all related to harmonics. The technical and financial ramifications of these harmonics have highlighted the need for efficient methods to keep harmonic distortions at the lowest levels and guarantee adherence to standard limits such as IEEE Std. 519 [2].

Energy is the lifeblood of the industry, and laborers are their muscles. Among the sustainability development goals (SDG), SDG 8 directs the use of technology to drive industrial transformation and sustainable production initiatives to support sustainable and responsible practices, including circular economy models, resource efficiency, and sustainable production and consumption patterns. Therefore, one aspect of corruption is using energy from dirty, expensive sources that increase carbon emissions rather than utilizing untapped, affordable, renewable, and clean energy. Scholars seek to recycle unutilized energy, which pushes the industrial community to present industries that rely on electricity generated from renewable sources (i.e., eco-friendly) to suppress carbon emissions and their related costs. However, there is a primary obstacle, which is Total Harmonic Distortion (THD) under different operating conditions is not treated, which neglects variations and uncertainties at the network level. Therefore, the suggested technique will be called Online harmonic identification technique (HIT) -in microgrid [3].

This system considers an innovation of circular economy aspects that interested by reduction of the wasted energy. The investment in energy will be reflected positively on the citizen satisfaction level because citizen satisfaction level (CSL) and related gross domestic product (GDP) per capita [4]. Egypt is a developing country that has subpar electricity sources, and relies on fossil fuels as a primary energy source which increases its ecological footprint and antagonizes the environment [4]. Therefore, the microgrid is the key to the success of this investment, especially if the charge station is designed to be a microgrid, according to the Online HIT technique. The proposed Online HIT is essential to meet power reliability, energy cost savings, environmental sustainability, energy independence, resilience, and electrification of isolated areas [5].

The article meets this goal by presenting a novel and accurate harmonic identification strategy for microgrids' controllers and distributed power systems based on many renewable energies. This strategy aims to upgrade Egypt to fore seats in export energy.

Microgrid controllers are independent energy systems that provide and track power to charging stations using one or more distributed energy sources (such as solar panels, wind turbines, combined heat and power plants, petrol or diesel generators, fuel cells, etc.). Many of the more recent microgrids also have energy storage built in, usually in the form of batteries, and some even have places where electric vehicles can be charged [6].

The proposed technique's main job is to maintain local grid stability (i.e., low levels of harmonic distortion) and save operating costs by allocating resources as cheaply as possible. In this work, the proposed technique manages two challenges and two suggested solutions. The first challenge is to observe and measure the THD fueled by various sources of microgrids connected by the main grid by Point of Common Coupling (PCC) while treating this distortion as accurately as possible in real-time via training observed data. The second challenge is its real-time power management system's capacity to adapt to any situation and obtain an energy management system's predictive approach, which reduces the prediction distortion.

Power continuity, even in a blackout, energy output, load consumption balance, and prompt analysis and decision-making in emergencies are all requirements for a microgrid system.

Figure 1 shows the equivalent circuit of the tested power distribution grid renewable. The time-varying currents introduced into the power network at the PCC to comprise the fundamental and harmonic components of power electronics-based applications of the main renewable sources including photovoltaic, wind and electric vehicles. Background harmonics typically linked to the power grid and originate from other electrically distant harmonic sources. The interactions between the state changes at the power network level and the harmonic sources, the developing harmonic distortions are computed solely from a harmonic source output current would not accurately reflect its actual harmonic distortions. To determine the actual share of each grid-connected system into harmonic-related concerns, the system operators monitor each system's harmonic performance under various operating conditions. However, obtaining true harmonic distortions requires a pure-sinusoidal voltage at the PCC [7], [8].

Numerous research studies on the extraction component for the individual and total of harmonic distortions' have been published in the literature such as harmonic impedance estimation [9], [10], critical impedance measurement [11], active and reactive power flow of harmonics [12], and the stochastic approach for harmonic estimation [13], [14], [15], [16]. The problem of estimating harmonic distortions has also been attempted to be addressed in several recent publications, as in [17], [18], [19], and [20]. However, to compute the harmonic distortions accurately, these methods necessitate prior knowledge about the network configurations and system components to develop dependable harmonic models. dealing with the hardness of transcendental nonlinear equations that characterize harmonic distortion, which is thought to be a

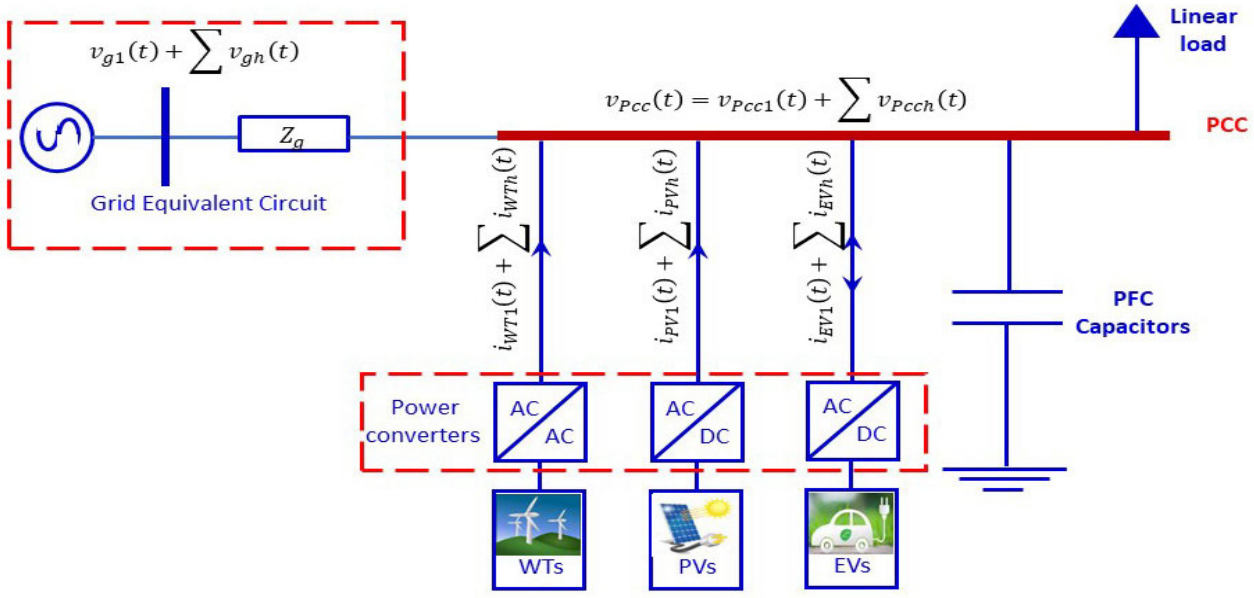

FIGURE 1. A diagram of recent electricity distribution networks.

complicated problem to solve, mainly when done in real-time. Because harmonic identification requires a large amount of memory and colossal processing time, it is one of the trickiest tasks in microgrids. Therefore, seeking to develop quick-analyzer algorithms is the main solution to present the Online HIT. The authors tackle their strategy using an Electric Transient Analysis Program (ETAP) simulator that can find both individual and total harmonic distortion from many harmonic sources and train the ANNs system and make its predictions better. The second solution is to develop a simulator program via Machine Learning Regression Analysis (MLRA), which is a type of artificial neural network (ANNs) system. Also, including location-specific data is proposed to address these complex issues.

The first solution to treating the first challenge relies on dealing with the hardness of transcendental nonlinear equations that characterize harmonic distortion, which is thought to be a complicated problem to solve, mainly when done in real-time. Because harmonic identification requires a large amount of memory and colossal processing time, it is one of the trickiest tasks in microgrids.

Regarding the extensively used of AI in harmonic distortion studies, some of researchers focused on reviewing these previous studies in [21], [22], [23], [24], and [25]. Moreover, the applications of ANNs and ANFIS in these tasks have been addressed. In [21], this study offers a thorough analysis of four of the most widely used CI-based optimization methods—fuzzy logic (FL), genetic algorithms (GA), ANNs, and ANFIS. It also covers each technique's fundamentals and its advantages and disadvantages. Swarm intelligence-based optimization techniques are not included in this study's scope or space analysis for the studied topic of study [21]. Also, in [22], a survey is given of the many artificial intelligence (AI) methods used in the study of harmonics, including decision trees, support vector machines (SVM), FL, and ANNs. In harmonic analysis, artificial intelligence systems fared better than conventional methods, especially when operating conditions varied. Improvements can yet be made in the areas of ensemble learning, training algorithms, optimal architectures, and additional comprehension as well as the application of combination approaches. In addition to outlining prospects for additional research on an increasingly significant subject, this review gives scholars knowledge about research patterns in harmonic evaluation [22]. Both conventional and contemporary (smart) harmonic estimation methods are thoroughly reviewed in [23]. New, clever AI techniques that are quick, precise, and effective have been examined as alternatives to address the problems with traditional estimation techniques. Researchers are increasingly using AI-based techniques because they can learn, forecast, and determine.

The recent development of Artificial Intelligence (AI) based systems, like artificial neural networks (ANNs), has spurred the interest of numerous researchers in the field of power electronics because of their ease of use, capacity for learning and generalization, and broad range of applications across multiple engineering domains. Numerous studies devoted to the estimation of PE harmonic performance [26] and active power harmonic filters [27] used ANNs systems. Additionally, due to the high computational burden of power networks, to assess the deviations of the fundamental and other harmonic content, an ANNs system was developed [28]. This system requires parallel processing operation. In [29], an ANNs-based intelligent harmonic estimation technique for power harmonic sources was presented. For estimating high-order harmonics, this solution produced

an extremely high error because it only used distorted voltage and current measurements. Although background harmonics can have a negative impact on the estimated distortions, a single harmonic source power system was taken into consideration.

To validate machine learning based on ANNs and ANFIS, it is obligatory to train with a massive amount of data to grantee their high accuracy in tests. A huge amount of data is produced by energy monitoring, particularly when it comes to harmonics at various locations over time. which need to be saved and used again, if possible. Most reviews concentrate on conformational measurements obtained at different sites, from which characteristic parameters are extracted. According to [30] and [31], For instance, three voltages, three currents, and ten-minute values of the harmonics 39 and 40 inter harmonics yield about $31X10^6$ data inputs per site after a year of observation. shows that a 2-year energy quality measurement campaign in 5 separate locations collected $250X10^9$ byte of data in total. While manual parsing can be done, it takes an exceedingly long time when dealing with multiple sites on measurements. Reference [32] states that patterns of daily variations in harmonic potential are matched between sites that use visual inspection to assess daily variations. an examination of how harmonics spread throughout a network when resonance is present. Reference [33] presents data on daily harmonic variations from several LV sites. The data is manually analysed, and patterns are found by visually examining harmonic currents against time, as described in paper [34]. An effort analysis was not submitted. The use of statistical analysis is more prevalent when dealing with multiple sites. As in [8] the analysis presentation scenario was repeated harmonics in different loading conditions by ETAP software program. The findings of the investigation are explained statistically across the various load conditions, primarily in the form of density function probabilities of voltage measurements for each harmonic order.

Three different systems were developed to extract the actual harmonic distortion of a nonlinear load in [35], [36], and [37]. Similar techniques were developed in [38], which used previous knowledge of the nonlinear load specifications and several ANNs for each harmonic component to forecast distortions in harmonics through equivalent coefficients. The proposed method used only identified the distortion limit in voltage and current signals and considered multiple time-invariant nonlinear loads.

Among many common applications for machine learning models, particularly in supervised machine learning, is the solution of regression problems. The relationship between independent and dependent variables is taught to algorithms through training. The model can then be used to fill in a data gap or forecast the result of fresh, unseen input data. Machine Learning Regression analysis is a method used to look into the relationship between features or independent variables and a dependent variable or result. It is a technique for machine learning predictive modelling, which makes use of an algorithm to forecast continuous outcomes [39], [40], [41], [42].

Regression models predict that the variables that are not dependent will influence the variables that are dependent [43], [44]. Reference [45] employs a regression approach to determine the value of the dependent variable, that known as ‘‘y,’’ based on the range of values associated with the independent variable, ‘‘x.’’ We address linear regression that more closely matches the predictive model in this paper [46]. There are three types of regression as stated in [47], Simple linear regression, multiple regression, and polynomial regression. A technique based on the Nonlinear Auto-Regressive Exogenous (NARX) neural network system was developed to estimate power harmonic distortions [41]. These suggested approaches, however, may fail to account for variations in the nonlinear load underestimation, that may result in an alternative harmonic effectiveness. As a result, the harmonic distortions may be inaccurately predicted for various operating conditions during the prediction phase.

On the contrary hand, [48] suggested a method for capturing the effect of time-varying nonlinear loads on harmonic performance. Numerous nonlinear loads are present in the work, but since the true harmonic distortions were overlooked, it is possible to assess the nonlinear loads’ influence on the PCC harmonic voltage distortions incorrectly. For solar PV systems, a power harmonic prediction system was created in [49]. The system solely forecasts the Total Harmonic Distortion (THD) under different operating conditions; variations and uncertainties at the network level were disregarded, and these should be considered for a precise and trustworthy estimation of harmonic distortions for a given application. Table 1 lists the established systems that have been documented in the literature along with the requirements, the harmonic distortions estimator’s capabilities and restrictions that has been proposed.

In [49] and [50], the suggested online harmonic mitigation technology improves the AC/DC voltage controller. It has two inputs that help manage well by adding a step-by-step pictorial sequence for the distortion’s value and the difference in accuracy between the reference signal and the actual signal to stop distortion. In [50], the suggested EV charging technique is integrated with this work to encourage building considerable investments in the EV industry and push towards electric public transportation, like the monorail, which is cheap and eco-friendly.

According to the best of the authors’ expertise here is no estimator of power harmonic distortions has been developed that considers changes in power network impedance states, interactions with additional harmonic sources and system components and the consequences of different operating conditions due to variations in renewable resources. To close this gap and predict harmonic distortions under a variety of operating conditions, this research project improves an ANNs-based enhanced harmonic distortions estimator system while taking location-specific data into account. The

TABLE 1. Statistics for the methods for calculating power harmonic distortion.

Technique	Ref.	Applications	Required data for training & test	Features/ limitations	
				Actual THD	DIFFERENT CONDITIONS
FL	[21-24]	Nonlinear Loads	PCC distorted current	Yes	No
GA, ANNs and ANFIS	[21,22]				
Machine learning	[23]	Power electronic converters	Inverter current harmonics between 2-150 kHz	Yes	Yes
ANNs, ANFIS	[29]	Power Harmonic Source	PCC Distorted voltage & Current	Yes	No
ANNs	[30,31]	Arc Furnaces	The harmonic 39 and 40 inter harmonics have three voltages, three currents, and ten-minute values.	No	Yes
ANNs	[34]	Desalination Water Plant	Bus distorted Voltage for harmonics 5,7,11,13,17,19,23 and 25.	Yes	Yes
MLP-ANNS	[35]	Nonlinear load	• Distorted voltage from PCC. • PCC distorted voltage with delay. • Non-linear load Curve	Yes	No
RNN	[36]	DC Drives	• PCC distorted voltage with delay. • Current nonlinear load.	Yes	No
ESN	[37,38]	AC Drives	• Distorted voltage from PCC. • Current with nonlinear load	Yes	No
NARX	[41]	AC Drives	• Distorted voltage from PCC. • Current with nonlinear load	Yes	No
ANNs	[48]	Nonlinear loads	Nonlinear loads that vary over time affecting harmonic performance	No	Yes
MLP-ANNs	[49]	PV Inverters	The amount of solar radiation. The inverter current's THD.[i]	Yes	Yes
MLRA	suggested approach	Renewable Energy Applications	• Wind speed or solar radiation. • Distorted voltage from PCC. • Distorted current in the system.	Yes	Yes

proposed system is expected to precisely determine the actual grid harmonic distortions that connected to multiple harmonic sources; power converter while accounting for harmonic emissions variations caused by power factor correction (PFC) capacitors, interactions with other harmonic sources, the intermittent nature of renewable resources, and system impedance changes. Using various harmonic sources that were taken from a test field and the IEEE 34-bus distribution test feeder, the suggested system will be verified. The IEEE 34-bus test feeder with confirmed harmonic sources verified the EATP results.

II. IMPROVEMENT OF THE HARMONIC ESTIMATING FRAMEWORK

This article encourages the integration of renewable energy sources to meet the sustainability of continuous productivity, which reflects positively on prosperity on distribution network that meets 2030 vision. It pushes us to pay attention to significant harmonic distortions when embracing today's power networks due to the use of power conversion systems, which are widely recognized as harmonic sources. Therefore, the users must take adequate measures to mitigate the technical and financial consequences.

A. AN ENHANCED HARMONIC ESTIMATING SYSTEM'S DEVELOPMENT

The ANNs are the popular substitute modelling technique for power system prediction applications. Multiple Linear Regression is used in this work to predict the actual infected harmonic current of a given harmonic source while avoiding interference with the grid, linked loads, or power sources. Figure 2 depicts the grid equivalent circuit with harmonics sources, PFC capacitors, additional linear/nonlinear loads, and the ANNs-based distortion caused by harmonics estimator. As a result, the distorted grid voltage, $v_{PCC}(t)$, is influenced by the actual and grid deliver harmonic portions of the PV inverter's distorted current, $i_{PV}(t)$, as well as the currents of other nonlinear loads/harmonic resources and background harmonics. The ANNs able to forecast the output signal $i_{estimated}(t)$, which represents the harmonic source distorted current when it is connected to pure sinusoidal, zero impedance infinite power source [49].

B. TRAINING ALGORITHM AND ANNs ARCHITECTURE

To enable the system to learn on its own from the majority of high-quality data, an ANNs harmonic identification algorithm is constructed by piecing together a parameterized module. To keep the system reliable, the primary task in this situation estimates the disturbance in supply voltages and compensate by injecting the voltage difference [50]. The most prevalent drawback of the classical method its need to linearization of nonlinear operating conditions that is cause the shortage in satisfying the target objective function.

The three primary neural electors that make up an ANNs technique are the input, hidden neurons, and output layer [3]. Inspired by the human brain, the ANN's components function in parallel. These layers represent the parallel information transmission caused by the interconnection of biological

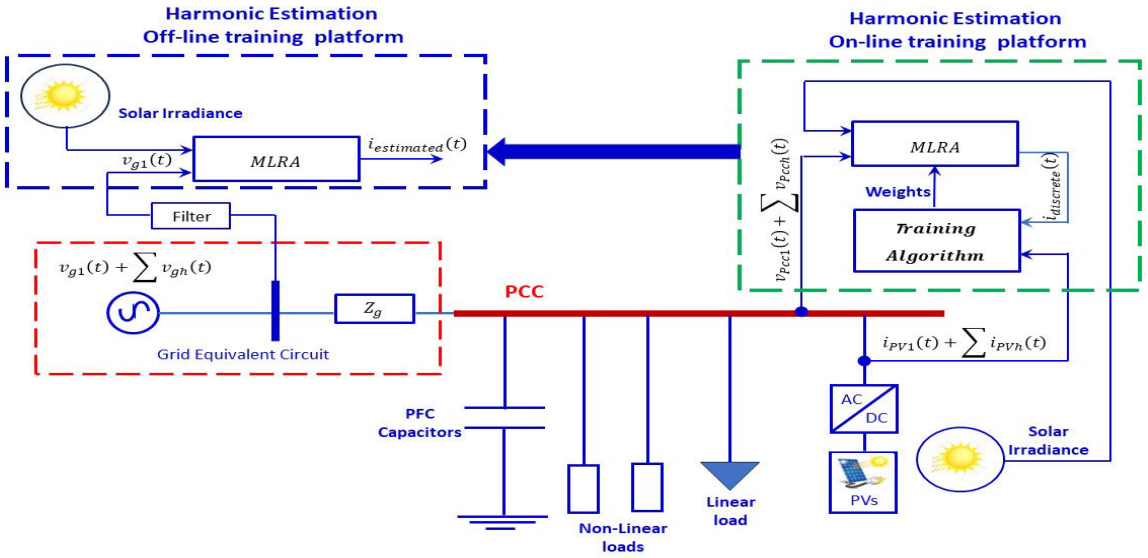

FIGURE 2. The grid equivalent circuit with harmonics sources and the MLRA-based harmonic distortion estimator.

neurons. Because of this feature, the system operates more quickly than it would if it used a sequential computation system. Furthermore, ANN's self-learning and adaptive qualities are employed to optimize the predicted and actual response error to improve the accurateness of prediction [51], [52]. The application of ANNs is motivated by its broad applicability in solving regression and classification tasks. The neural network functions as a black box because it does not need any specific system information. The feed-forward back-propagation approach is the most appropriate among all neural network architectures for solving non-linear problems.

It is difficult to predict which version of the training algorithms will run most efficiently for a given problem. This is due to a variety of features, with the problem level of difficulty, the large amount of data in the training phase, the biases and weights numbers in a particular assembly, the effectiveness of the target error, and the network's objective, such as approximation of functions or recognition of patterns [53]. In the literature, many technically prompted algorithms have been adjusted to train the ANN, the widely one that is merited by its low computational effort and high convergence rate and called as Levenberg- The feed-forward pack propagation architecture is shown in Fig. 3.

The MSE and RMSE provided in Eqs. (1) and (2), respectively, are used to verify the ANNs model's performance measurement. Equation (1), which represents the network's output value of 0.0001, shows how the weight and bias are adjusted for the network mean square error (MSE) value. The ANN-BP algorithm's prediction of the target weight value is based on the smallest mean square error estimation, which measures its effectiveness [54].

$$MSE = \frac{1}{n}\sum_{i=1}^{n}\left(\mathcal{Y}_i - \hat{y}_i\right)^2 \tag{1}$$

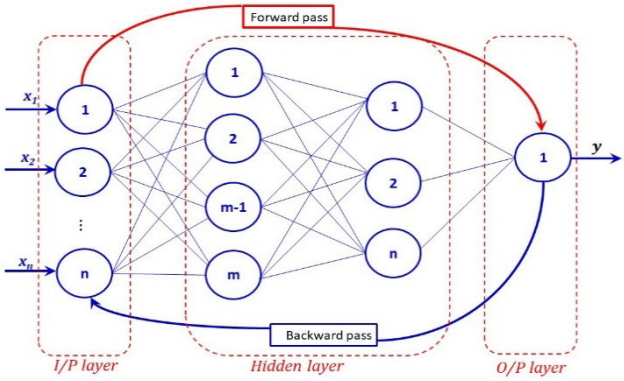

FIGURE 3. ANN feed-forward back-propagation construction.

$$RMSE = \sqrt{\frac{1}{n}\left(\sum_{i=1}^{n}\left(\mathcal{Y}_i - \hat{y}_i\right)^2\right)} \tag{2}$$

where,

n: the input data sets signify number
$\hat{y}_i$ the harmonic distortion response
$\mathcal{Y}_i$ the forecast harmonic distortion response

Sequential equations with numbers for each equation in a neural layer, every neuron takes a weighted set of inputs and produces an output. An Artificial Neuron's (AN) activation potential (Ai) can be stated as follows:

$$A_i = \sum_{j=1}^{N} w_{ij}x_j - bo_j \tag{3}$$

where,

N: the input number vector parameters x_j
w_{ij}: the interconnected weight matrix
b_{oj}: the number of neurons "bias" vector

By adjusting the bias coefficient, the activation signal is regulated [55]. The local information that is stored in the neuron and is either internally available or received through the weighted coefficient determines the output of the neural layer. To produce the best forecasting ANNs model, the sigmoid transfer function is used in the training mechanism in this paper. In mathematics, the sigmoid function is expressed as:

$$\emptyset\,(x) = \frac{1}{1 + e^{-kA}} \tag{4}$$

where,

$\phi(x)$: the sigmoidal activation functions
k: the curve control parameter

The sigmoid function used in the hidden layer and required for the weight rule updating is given in Eq. (4). Any continuous function can be approximated with the sigmoidal activation function $\phi(x)$ to any desired level of accuracy. The Levenberg-Marquardt optimization technique, which is characterized by the performance index defined in Eq. (5) [55], is used to improve the prediction performance through backpropagation.

$$F\,(w) = \sum_{p}^{p=1}\left[\sum_{k=1}^{k}\left(d_{kp} - A_{kp}\right)^2\right] \tag{5}$$

where

w: a combination of the weight vectors
d_{kp}: the expected value of the kth response and the nth pattern
A_{kp}: is the measured value of the kth response and the nth pattern
p: the number of the patterns and k stands for output elements

As demonstrated in Eq. (6), the shifting between gauss newton and error back-propagation is effectively controlled by the Levenberg Marquardt back-propagation (LMBP) learning rule with coefficient μ.

$$\Delta w = \left(J^T J + \mu I\right)^{-1} J^T e \tag{6}$$

where,

μ: the algorithm's scalar controlling parameters
e: the error
J: The Jacobian matrix with error vector

The value of μ rises with each iteration's increase in error and falls with each step reduction in error (e). The Jacobian matrix with error vector [J] is described by Eq. (6). In Eq. (7) the Jacobian Matrix is explained.

$$[J] = \begin{pmatrix} \frac{\partial F\,(x_1, w)}{\partial w_1} & \cdots & \frac{\partial F\,(x_1, w)}{\partial w_w} \\ \vdots & \ddots & \vdots \\ \frac{\partial F\,(x_N, w)}{\partial w_1} & \cdots & \frac{\partial F\,(x_N, w)}{\partial w_w} \end{pmatrix} \tag{7}$$

With the learning rate set to 0.001, this LMBP achieves a faster conversion rate, allowing the network to reach the target error of $1e^{-15}$. When the chosen MSE criterion is satisfied with increased accuracy, a network is said to have converged. The fundamental formulas used to calculate the Toal Harmonic Distortion is outlined in the following equation:

$$THD_b = \frac{\sqrt{\sum_{h=2}^{H}\left|Vbus_b^h\right|^2}}{\left|Vbus_b^1\right|} \tag{8}$$

where,

H: Maximum considered harmonic order;
$Vbus_b^h$ Voltage at bus b for harmonic order h;
THD_b THD at bus b.

C. ONLINE HARMONIC IDENTIFICATION MODELLING BASED ON MACHINE LEARNING REGRESSION

In the following section, a brief discussion about the different regression models will be illustrated as:

1) SIMPLE LINEAR REGRESSION

A case study with a single independent variable is so-called a simple linear regression [56]. The variable's dependence is defined through simple linear regression.

$$y = \beta_0 + \beta_1 x + \varepsilon \tag{9}$$

where,

y: the estimated dependent variable score
β_0: a constant
β_1: the regression coefficient
x: the score on the independent variable

The impact of independent variables is separated from the interaction of dependent ones through simple regression [57].

2) MULTIVARIATE LINEAR REGRESSION (MLR)

The Multivariate Linear Regression (MLR) is a statistical method that predicts the output based on several explanatory variables. In [57], the aim is identified to find linear input/output model.

$$y = \beta_0 + \beta_1 x_1 + \ldots + \beta_m x_m + \varepsilon \tag{10}$$

where,

y: the estimated dependent variable score
β_0: a constant term (intercept)
$\beta_1, \beta_{2\ldots}, \beta_m$: the regression coefficient that determines the slope of the trend surface.
$x_1, x_2 \ldots, x_m$: the score on the independent variable

Equation (11) determines the formula matrix [43] as:

$$\hat{\beta} = (X^T X)^{-1} X^T y$$

$$\beta = \begin{bmatrix} \beta_0 \\ \beta_1 \\ \vdots \\ \beta_2 \end{bmatrix}, \; X = \begin{bmatrix} 1 & x_{11} & x_{12} & \cdots & x_{1m} \\ 1 & x_{21} & x_{22} & \cdots & x_{2m} \\ \vdots & \vdots & \vdots & \vdots & \vdots \\ 1 & x_{n1} & x_{n2} & \cdots & x_{nm} \end{bmatrix}, \; Y = \begin{bmatrix} Y_1 \\ Y_2 \\ \vdots \\ Y_n \end{bmatrix} \tag{11}$$

3) POLYNOMIAL REGRESSION

Polynomial regression [58], [59] is a regression analysis procedure that examines the relationship between input and output variables using nth degree polynomial modelling. In polynomial regression, the data polynomial equation combines with the curvilinear interaction of the dependent/independent variables, a special case of maximum likelihood regression [60]. The polynomial model [61], [62] looks like:

$$y = \beta_0 + \beta_1 x + \beta_1 x^2 \ldots + \beta_h x^r + \varepsilon \tag{12}$$

where,

r: An integer numbers that denotes the degree of the polynomial.

In this research, the suitable regression model for the nature of the problem is the linear regression (LR). One technique for using linear regression is called least squares. It assists us in identifying anomalies in our data and making predictions about the future based on an existing set of data. Values that are too good or bad to be true or that indicate exceptional circumstances are known as anomalies. In the following a brief overview of least square technique will be demonstrated.

a: LEAST SQUARE TECHNIQUE

Using the Least Squares Method (LSM) [65], [66], it can determine which curve or line best fits a given collection of variables by minimizing the offsets squares (residual portion) of the curve's points. The linear regression model employs the LSM to determine the coefficients b_0 and b_1 in order to minimize the sum of the squared distances between actual value *yi* response from the following equation:

$$\hat{y} = \beta 0 + \beta 1 x_i \tag{13}$$

$$(b_0, b_1) = arb \min_{(\beta_0, \beta_1)} \sum_{i=1}^{n} [\beta_0 + \beta_1 x_i]^2 \tag{14}$$

Indicate that the solutions are b_0 and b_1.

$$b_1 = \frac{\sum_{i=1}^{n} (y_i - \bar{y})(x_i - \bar{x})}{\sum_{i=1}^{n} (x_i - \bar{x})^2} = \frac{S_{xy}}{S_{xx}} \tag{15}$$

$$b_0 = b_0^* - b_1 \bar{x} = \bar{y} - b_1 \bar{x} \tag{16}$$

The smallest of all regression coefficients between β_0 and β_1.

The LSM goal is to identify the accuracy of the estimated parameters by applying the least squares that is the closest line to all points (x_i, y_i).

In this paper, the aim is to minimize the squares of the standard linear regression technique.

$$\frac{\partial}{\delta \beta_0} \sum_{i=1}^{n} \left[y_i - (\beta_0 + \beta_1 x_i) \right]^2 = 0 \tag{17}$$

$$\frac{\partial}{\delta \beta_1} \sum_{i=1}^{n} \left[y_i - (\beta_0 + \beta_1 x_i) \right]^2 = 0 \tag{18}$$

The regression can be used line $= \beta_0 + \beta_1 x_i$, which is conventionally indicated, to characterize the relationship between x and y given that b_0 and b_1 are the solutions to the system. Using a centralized linear model makes solving for b_0 and b_1 simpler:

$$y_i = \beta_0^* + \beta_1 (x_i - \bar{x}) + \varepsilon_i \tag{19}$$

where $\beta_0 = \quad \beta_0^* - \beta_1 (\bar{x})$. we need to solve for

$$\frac{\partial}{\delta \beta_0} \sum_{i=1}^{n} \left[y_i - (\beta_0^* + \beta_1 \bar{x_i}) \right]^2 = 0 \tag{20}$$

$$\frac{\partial}{\delta \beta_1} \sum_{i=1}^{n} \left[y_i - (\beta_0^* + \beta_1 \bar{x_i}) \right]^2 = 0 \tag{21}$$

By calculating the partial derivatives concerning $\beta 0$ and $\beta 1$.

$$\sum_{i=1}^{n} \left[y_i - \left(\beta_0^* + \beta_1 (x_i - \bar{x}) \right) \right] = 0 \tag{22}$$

$$\sum_{i=1}^{n} \left[y_i - \left(\beta_0^* + \beta_1 (x_i - \bar{x}) \right) \right] (x_i - \bar{x}) = 0 \tag{23}$$

$$\sum_{i=1}^{n} y_{i=n\beta_0} + \sum_{i=1}^{n} \beta_1 (x_i - \bar{x}) = n\beta_0^* \tag{24}$$

Therefore, we have $\beta_0^* = \frac{1}{n} \sum_{i=1}^{n} y_i = \bar{y}$ Substituting β_0^* by $\bar{y}$ leads to the following equation:

$$\sum_{i=1}^{n} [y_i - (\bar{y} + \beta_1 (x_i - \bar{x}))] (x_i - \bar{x}) = 0 \tag{25}$$

The LSM's rationale is to compute estimation of parameters by selecting the row that is ''closest'' to each and every data point (x_i, y_i) [65]. In regression analysis, residual analysis is essential. For the measurements *yi* and the fitted values $\hat{y}_i' s$, residual linear regression can be found, and residuals can be displayed. It needs to be Recalling that the regression model does not contain the ε_i term as a result, no regression error is found, and remaining regression is identified [66]. The expected value, or the population average, is typically not observed [67], [68]. The description of a test using a linear regression model is represented as: -

b: F-TEST

The F− test is denoted in Eq. (26) [69] as the most more reliable than the other tests.

$$F = \frac{\sum \left(\hat{y}_i - \bar{y}_i\right)^2 \Big/ (m-1)}{\sum \left(y_i - \hat{y}_i\right)^2 \Big/ (m-1)} \sim F(m-1, n-m) \qquad (26)$$

where the degree of freedom in modifying regression is denoted by (m-1). $\sum \left(\hat{y}_i - \bar{y}_i\right)^2$; $n - m$ is the residual variation's degree of freedom $\sum \left(y_i - \hat{y}_i\right)^2$.

If $F\alpha F$ *(m-1, n-m)*, then A significant linear relationship exists between the variables y and x_1, x_2, $\ldots x_m$ is less than the priority rate of α, the regression equation is deemed significant; conversely, it is not significant.

c: t-TEST

Determine whether the independent variable's impact on y is relevant and in line with the test hypothesis. Test variable t in statistics [70]:

$$t_j = \frac{\hat{\beta}_j}{\sqrt{c_{jj}}\sqrt{\frac{\sum (y_i - \hat{y}_i)^2}{(n-m)}}} \qquad (27)$$

where Cjj is the jth component on matrix $(x'x)^{-1}$

III. POWER MODEL INVESTIGATION

Figure 4 depicts three-phase power system in a single-line diagram. The system consists electrically linked to two PV systems, WT, a nonlinear load, and capacitors, and an equivalent voltage source after an impedance to simulate a power grid. The Appendix contains the system specifications.

A. THE MODELLED POWER SYSTEM'S DESCRIPTION

The Electric Transient Analysis Program (ETAP) is used to simulate the power system in order to investigate the harmonic accomplishments of power electronics-based applications and their interactions with other components of the system under various power events. Since it is assumed that the three-phase system is balanced and symmetrical, current and voltage measurements in a single phase are shown along with the corresponding distortions.

B. HARMONIC PERFORMANCE OF THE MODELLED SYSTEM

In steady state mode, the solar PV-1 system is being assessed, the PV-2 and wind turbine during the simulation interval. The solar PV-1 system uses 1000 W/m^2 solar radiation at 35°C ambient temperature while the wind turbine system operates at 12 m/sec wind speed. The mathematical model includes multiple states of power network events as well as two solar radiation profiles in order to examine Effects of network level changes and solar irradiance fluctuations on photovoltaic power generation PV-1 systems' harmonic performance and PCC voltage.

The grid impedance (Zg) rises up to 25% gradually, the nonlinear load increases by 60 % step by step and the PFC capacitor disconnects at some cases to obtain substantial number of cases to train the model. Additionally, two different solar irradiance profiles of the solar PV-1 system are considered. For example:

In Profile 1, the solar irradiance to be 800 W/m^2 at 1 sec. and the outside temperature twenty five °C.

In Profile 2, There is a 1000 W/m^2 solar irradiance and a twenty five °C outside temperature at one second.

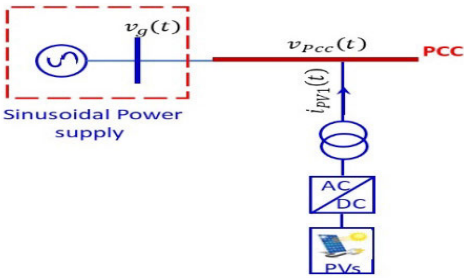

FIGURE 4. A pure sinusoidal source drives the solar photovoltaic system.

Moreover, the use of such simulation tools is useful when sinusoidal voltages are supplied to the PCC. This performance will be achieved by blocking other harmonic resources and reducing the network impedance to close to its lowest value (Zero). By using the ANNs-based harmonic estimator, one can compare the harmonic performance of an individual solar PV-1 system. Figure 4 shows a photovoltaic PV-1 system linked to a pure sinusoidal power source. Different scenarios will be taken into consideration d in the following subsections for the simulated system.

Case Study 1 (PCC Voltage Distortion with Profile 1): To simulate the system, Profile 1's solar irradiance is used for PV-1 systems, and power events are considered for all appliances connected to the grid. The outputs are illustrated in Figure 5. The module was evaluated at a nominal solar radiation and an ambient temperature of 800 W/m^2 and 25 °C, respectively.

Case Study 2 (PCC Voltage Distortion With Profile 2): Similar to Case 1, but in this instance, the solar PV-1 system uses Profile 2. Figure 6 shows the results in this case. It was assessed with an ambient temperature and rated solar radiation of 25 °C and 1000 W/m^2.

Case Study 3 (PCC Sinusoidal Voltage With Profile 1): Connecting a photovoltaic PV-1 system exclusively to an ideal power source is not feasible in real domain systems. Instead, solar radiation from Profile 1 is simulated. Figure 7 shows the corresponding simulation results.

Case Study 4 (PCC Sinusoidal Voltage With Profile 2): Independent connections are made between the PV-1 solar power systems to ensure the optimal power source; however, in this instance, Profile 2's solar irradiance is utilized. The application of the FFT solution to corresponding remnants with regard to the fundamental frequency during the simulation period results in this expression for the THD

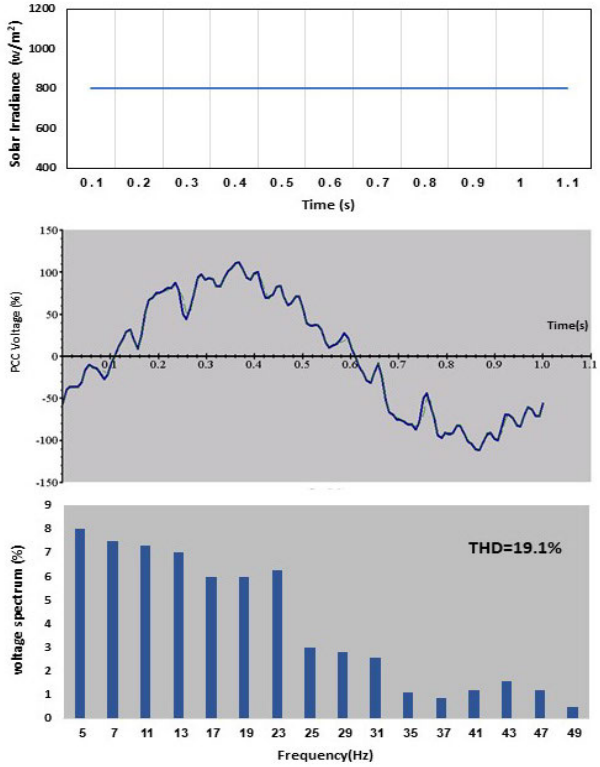

FIGURE 5. THE module was evaluated at an ambient temperature of 25°C and a nominal solar irradiance of 800 W/m^2.

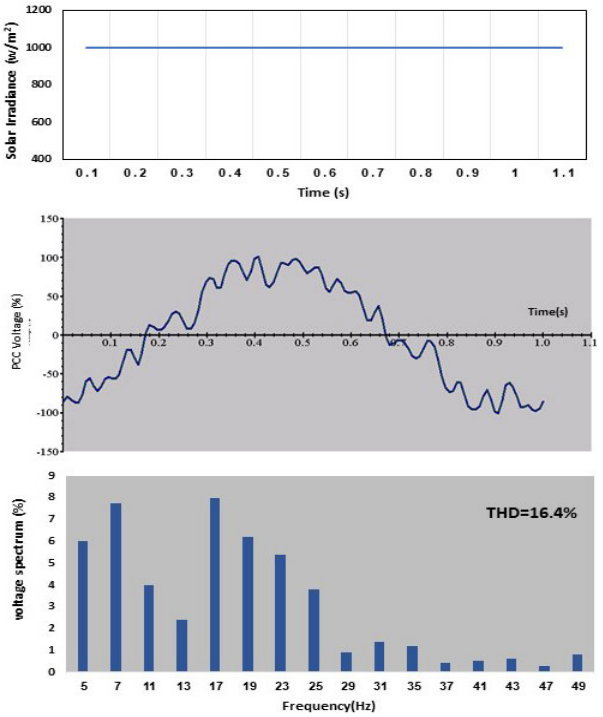

FIGURE 6. the results in this instance, a nominal solar irradiance of 1000 W/m^2 and an ambient temperature of 25°C.

output current and PCC voltage of the exit PV-1 system. The simulation results for Cases 1-4 are shown in Figures 5-8,

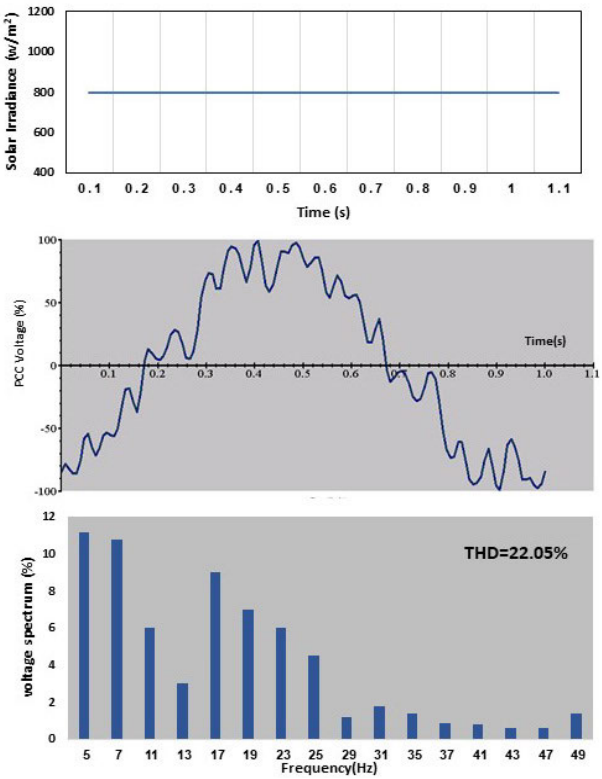

FIGURE 7. The module was evaluated at an ambient temperature of 35°C and a nominal solar irradiance of 800 W/m^2.

respectively. The main observation from these figures can be expressed as follows:

- When compared to Cases 1 and 2 with an ideal power source, sources of harmonics and power events typically of a noticeable impact on both the PV-1 inverter harmonic emissions and the grid voltage and lead to inaccurate estimation.
- It is evident that the solar PV-1 system's PCC voltage THD follows an inverse relationship with the profile of solar irradiance. For instance, Case 1 experiences a decrease of 2% in the PCC voltage THD as a result of an increase of 200 W/m^2. This highlights how the THD depends on the operating circumstances, as was covered in [49].
- However, as also mentioned in [7] and [49], the power events may have little effect on the solar PV output current THD due to Profile 2's constant variations in solar irradiance.
- There has been a notable decrease in the voltage distortions at the PCC from 19.1% to 16.4% in Cases 1 and 2, as a result of the rise in nonlinear loading level.
- Additionally, a 20% increase in network impedance increases the THD of the PCC voltage from 18% to 22.05% and leads to an increased voltage drop for each harmonic component.
- Synchronous circuits and control systems are extremely sensitive to grid voltage distortions in grid-connected

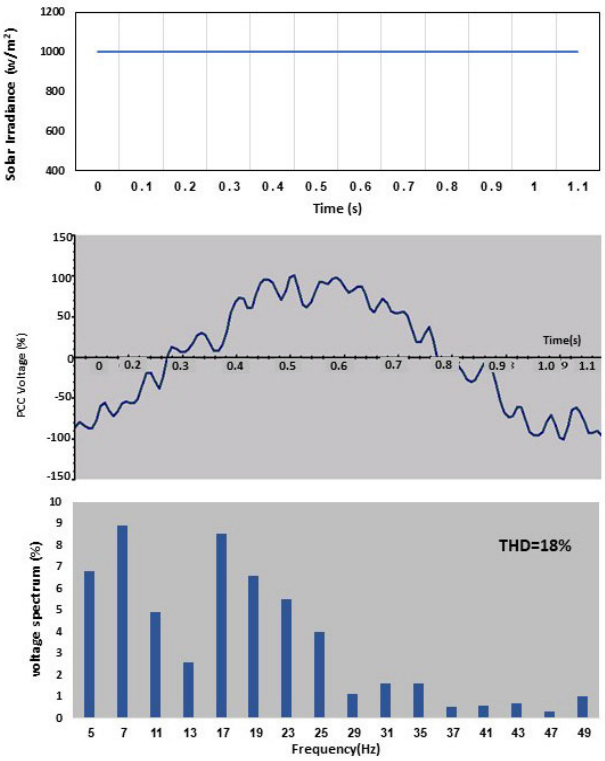

FIGURE 8. The results in this instance, a nominal solar irradiance of 1000 W/m^2 and an ambient temperature of 35°C.

PE-based applications [7], [71], [72]. Therefore, in case two, the waveform distortion of the PV system increased due to the increase in PCC voltage distortion.

- Due to the interaction between the PFC capacitance, other system components, and the inductive elements of the network, PFC capacitors typically cause undesirable amplification effects on harmonic components within the resonance point. When the PFC capacitor is disconnected, the resonance disappears, resulting in a three. One percent increase in the PCC voltage THD of the PV system.
- As solar irradiance changes with a pure sinusoidal voltage, the actual THD of the current in a solar PV-1 system is significantly lower than when supplied with a PCC when supplied distorted voltage.
- It can be observed that the suggested ANNs-based harmonic estimator is then trained and evaluated using the outcomes of the simulated system. In other words, the suggested harmonic distortions estimator will be trained using Case one second time-varying solar irradiance over the simulation period, along with the voltage and current that correspond to it. We then use the simulation software results for cases 3 and 4 to evaluate the performance of the ANNs-based harmonic estimator over a range of solar irradiation points. It is worth noting that the ANNs system works well with signals rescaled within ±1%. Due to the nature of the neuron's activation function [73], the voltage percentage results shown in Figures 5-8 were applied without the need for rescaling. However, the solar radiation is readjusted to the nominal value of 1000 W/m^2.

IV. EVALUATION OF ESTIMATORS' PERFORMANCE AND TRAINING

Renewable energy-based power sources, such as solar PV systems, are associated with inherent uncertainties caused by partial/complete shading and faulty cells/panels, which must be addressed for reliable estimation. Furthermore, to ensure reliable and robust estimating performance, the fault tolerance of such an ANNs estimator should be investigated. It is also worth noting that advances in neural networks, such as deep neural networks, may be possible for large-scale data-processing applications. This section aims to evaluate the estimator via discovering its data relationships significant to train it as will discuss in section V, subsection A.

A. ANNs TRAINING PHASE

MATLAB (R2022b) is utilized to develop the ANNs system depicted in Figure 3 on a computer equipped with a 64-bit Windows 8 operating system, an Intel Core i5 and RAM of 16 GB. The system is trained using the Levenberg-Marquardt backpropagation algorithm. Because of the constant decline in Profile 2's solar irradiance, The ANNs system is trained using the voltage, current, and solar radiation simulation results of case two. In the training stage, a predetermined range of the system output results are processed in order to examine the performance of the suggested estimator.

The distorted wave's half cycle is first sampled at 17 separate points spaced regularly along the time axis and encompassing solar irradiances ranging from 800 to 1000 W/m^2. Without performing any pre-processing, the feed-forward neural network receives these sampled values at each bus as input signals. The literature suggests that the harmonic distortion estimate, which is based on an ANNs model, would be suitable for a multilayer perceptron through eight inputs, two hidden layers and one output.

For ANNs systems, a low MSE value is typically sufficient in a variety of applications. Nonetheless, in order to avoid misestimating the actual distortion value when using the ANNs system, a low degree of accuracy is required in the harmonic distortion estimator. Despite this, the number of neurons in the hidden layer is chosen due to his MSE observations, which results in five times the total number.

There are 170 sets of vectors in the database; 70% of them are simulation data vectors that obtain a low enough training error, and 15% of sets of vectors are kept for the validation stage. and the rest 15% are kept for test step. The ANNs training parameters are compiled in Table 2.

For ANNs systems, a low MSE value is typically sufficient in a variety of applications. Nonetheless, in order to avoid misestimating the real distortion when using the ANNs system, the error of the harmonic distortion estimator must be as

TABLE 2. ANNS training parameters numbers.

Inputs No./ bus	20	Outputs No.	1
training samples	170	training parameters.	84
Hidden layers	2	training Epochs	1000
No. of neurons for the two hidden layers	25, 14	Target error	1×10^{-3}

low as possible. For the lowest MSE of 2.05e-06 as shown in Fig. 9.

The number of neurons in the hidden layer is dependent on the network's ability to generalize the recognition process. Twenty-five neurons in the first hidden layer and fourteen in the second hidden layer are the optimal numbers for the network's harmonic components. However, using fifty neurons in the first layer and fourteen neurons in the second hidden layer gives a little bit of error compared to 25, 14 neurons in the first and second layers hidden, respectively. Fig. 9 shows a comparison between the two models to determine the optimal number of neurons in the hidden layers. Eventually, the activation functions for the two hidden layers will be sufficiently strong to saturate. These functions are sigmoidal and linear for each layer of training algorithms. Table 3 depicts the ANNs training progress and different ANNs parameters.

This is primarily due to the large amount of data in the training set and the prominent level (precision) required for this type of application, which results in an extremely considerable number of neurons.

The fitting of the ANN's output signal (shown in blue) to the solar PV-1 system's simulated (shown in doted green) in Case 2.

B. ANNs TEST PHASE

In this section, the performance of the ANNs expert system is evaluated for different solar radiation values within the training stage. An expert ANNs system written in MATLAB receives a vectorized signal of solar radiation and a pure sinusoidal voltage signal with a mathematically generated percentage amplitude. The separately simulated system for the same solar radiation and sinusoidal PCC voltage is contrasted with the expected results, as demonstrated in Figure 10. ANNs systems process input and output signals as samples and produce simulation results that are stable over simulation time. When sunlight is within the training range, the expert ANNs has reliable performance. When the expert ANNs system is given the pure sinusoidal voltage signals in Figures 11 and 12 for solar sunlight values of 800 W/m^2 and 1000 W/m^2, respectively, the predictions representing the estimated actual harmonic distortion of the system the signals show good agreement. As in Cases 1 and 2, we simulated an ideal power supply connected system. The FFT solution for the two signals was completed in MATLAB with a maximum error of approximately 18%.

The results highlight the accuracy of the ANNs system regarding each important harmonic component. The THD of the predicted signal is another metric used to evaluate how well the proposed ANNs-based harmonic distortion estimator performs. The proposed estimator's performance was trained and optimized using the results of a simple energy system simulation as IEEE standard limits.

A second criterion for the THD of the predicted signal is the proposed harmonic distortion estimator, which is based on an ANNs algorithm. The simulation of a simple energy system was used as 'reference' and the IEEE standard limits to train the proposed estimator, and then to improve upon it. It is anticipated that the ANNs harmonic distortion estimator will produce harmonic performance results for a solar system inverter when connected to purely sinusoidal power, with actual harmonic emissions being more accurate. Table 4 displays the THD deviation for both the actual and predicted signals. This is calculated using the following formula:

$$error(\%) = \frac{THD_{actual} - THD_{predicted}}{THD_{actual}} \times 100 \qquad (28)$$

A small variation exists between the simulated and predicted THD. The explanation for this is the non-zero ANNs performance error, which arises from the featureless harmonic components of each predicted signal generated by the proposed estimator. The expert ANNs' perform better when exposed to sunlight in the training area. In Figures 11 and 12, when a pure sinusoidal voltage signal is applied to the expert ANNs system, the predicted signals for solar irradiance values of 800 W/m^2 and 1000 W/m^2, respectively, are in good agreement with the simulated signals. The systems in Case 2 and Case 4 are connected to an ideal power supply, and the actual harmonic distortion of the system is less than the estimated value. The ANNs system's precision regarding the significant harmonic components was demonstrated through FFT analysis in MATLAB, with an error limit of approximately 0.78 %.

The computational cost of an ANNs system with different numbers of neurons is a crucial factor to consider during the training and prediction stages. Convergence requires more computation time when there are more neurons in the hidden layer for a given data size. But in the proposed algorithm the training and forecasting processes took about 3 hours and 11 minutes, respectively, this represents a computational burden. Computers with high computational capabilities can further reduce it. More memory and capacity to process substantial amounts of data.

C. MLRA TRAINING PHASE

MLRA employs the linear regression algorithm to train the system. Because the solar radiation in profile two is decreasing all the time, the linear regression in CASE 2 is trained using simulated voltage, current, and solar radiation. During the training phase, a predefined range of system output results is processed to evaluate the performance of the proposed estimator. During the training phase, a pre-defined range

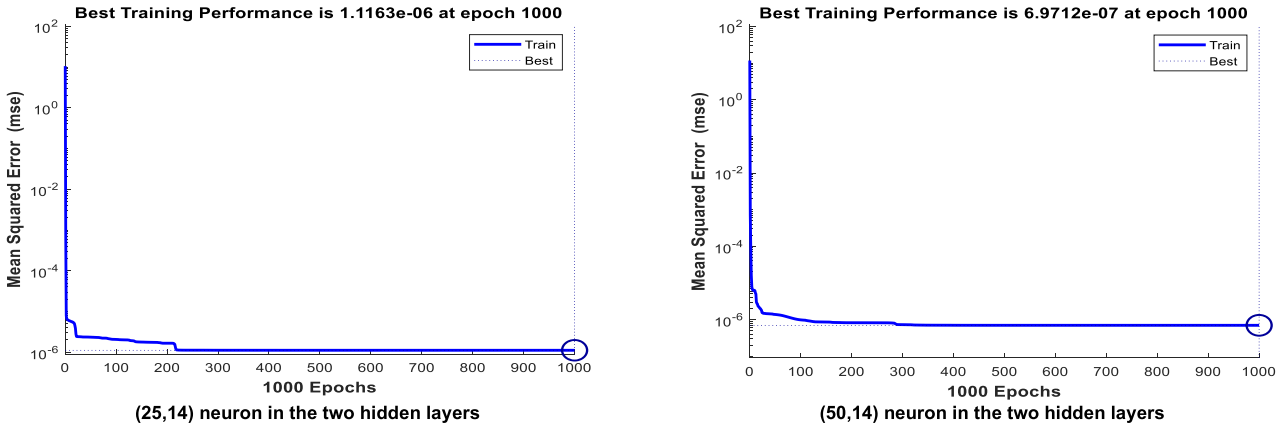

FIGURE 9. The MSE during the training phase with different neurons in hidden layer.

TABLE 3. ANNs training progress.

Unit	Epoch	Elapsed Time	Performance	Gradient	Mutation	Validation Checks	Training Time (hh:mm: ss: ^{oo})
Initial Value	0	-	7.39	22.2	0.001	0	03:101:54
Current Value	1000	03:11:54	$7.77e^{-07}$	$2.05e^{-06}$	$1e^{-11}$	0	
Objective Value	1000	-	0	$1e^{-15}$	$1e^{+120}$	18	

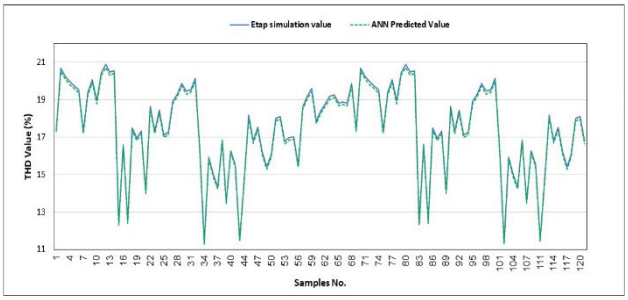

FIGURE 10. The PCC voltage THD comparison between experimental and the ann predicted results for training samples.

TABLE 4. THD error between the actual and predicted signals.

Solar radiation	1000 W/m^2	800 W/m^2
Simulated PCC voltage THD	16.4%	19.1%
Simulated PCC voltage THD	16.29%	18.95%
Error	0.67%	0.78%

of ETAP outputs are then processed for testing using the proposed estimator.

The half-cycle of the distorted wave was sampled at 17 discrete points regularly spaced along the time axis and including solar irradiances ranging from 800 to 1000 W/m^2 based on the fundamental frequency, as in the ANNs. The feed-forward neural network receives these values sampled in each vector as input signals without preprocessing. The linear regression machine learning system, as previously discussed in the literature, produces superior results when using MLRA.

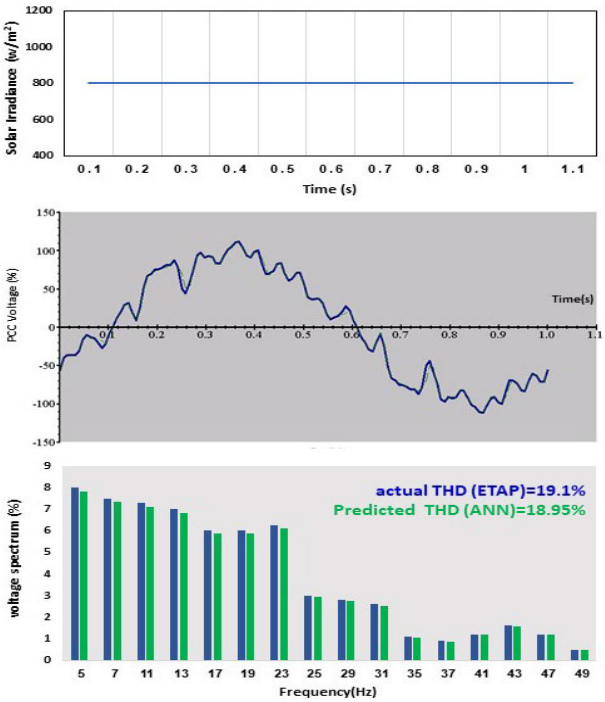

FIGURE 11. The performance of proposed approach as in profile 1 (800W/m^2).

In many applications, a minimum RMSE value is sufficient for MLRA systems. However, to avoid overestimation of the true deformation when using an MLRA system, the harmonic deformation estimator should be as accurate as possible. Figure 13 depicts the selection of several MLRA algorithms

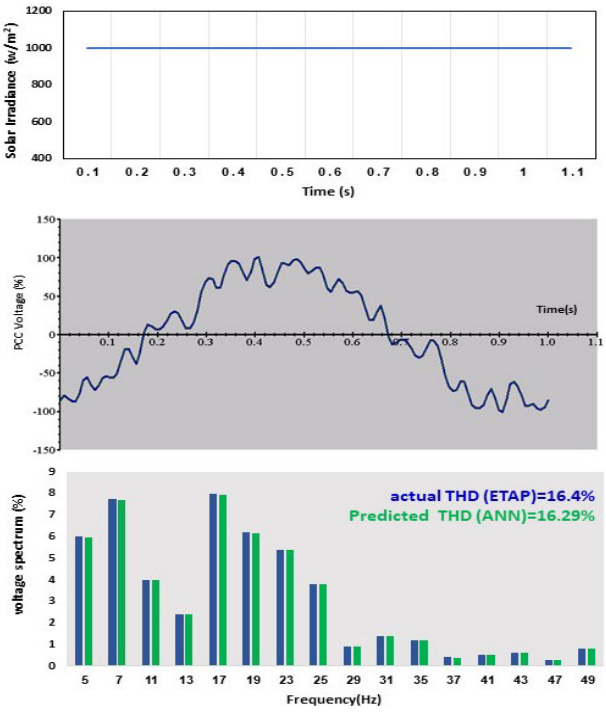

FIGURE 12. The proposed method's performance as in profile 2 (1000 W/m^2).

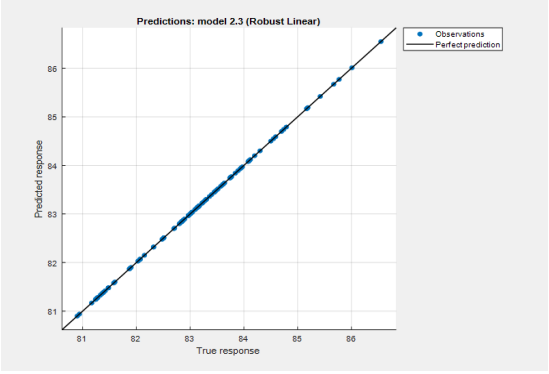

FIGURE 13. The prediction response for the robust linear regression model.

for the minimum RMSE value obtained from Linear regression under MATLAB program. It determines the network's ability to generalize the detection process. Table 5 displays the MLRA training progress among various models.

Among the 26-machine learning linear regression models, a low RMSE value is sufficient for Machine Robust Linear Regression model as shown in Table 5, the blue highlighted row (the fourth row). However, in order to avoid underestimating the true distortion when using the ANNs system, the harmonic distortions estimator must have the lowest possible error. The database contains 170 sets of vectors; 70% of them are simulation data sets with a low enough training error, and 15% are kept for the validation stage. The remaining 15% is set aside for the testing phase.

Table 6 lists the optimal LR training parameters. Also, Fig. 13 depicts the prediction response for the Robust Linear Regression model.

D. MLRA TEST PHASE

The performance of optimal Linear Regression model is evaluated in this section for various solar irradiance points within the training range. The expert MLRA system created in MATLAB is fed a vectorized signal of solar irradiance and a generated pure sinusoidal voltage signal. The expected results are then compared to the independently simulated system results for the same solar irradiance and sinusoidal PCC voltage, as shown in Fig. 4. The MLRA model samples its input and output signals at a constant rate in relation to simulation time and generates simulation results. When the solar irradiance is within the training range, the optimal MLRA performs well. When an expert MLRA model is given a pure sinusoidal voltage signal in Figures 11 and 12, for the two aforementioned profiles (Profile 1 and Profile 2), respectively, the predicted signals, which represent the true harmonic distortion of the system under estimation, show good agreement with that of the simulated system connected to an ideal power source, as in Cases 1 and 2. In MATLAB, the FFT solution for the two signals was completed with a maximum error of about 21%. The results demonstrate the MLRA model's high accuracy for each significant harmonic component. Another metric used to evaluate how well the proposed MLRA-based harmonic distortions estimator performs is the THD of the predicted signals. The proposed estimator's performance was trained and optimized using the results of the simple power system simulation as a benchmark and guide.

The THD of the predicted signals is another metric for assessing the performance of the proposed ANNs-based harmonic distortions estimator. The results of the simulated simple power system were used as a benchmark and reference to train and optimize the proposed estimator's performance. The MLRA harmonic distortion estimator is expected to produce the same results of the PV inverter harmonic performance when connected to a pure sinusoidal power source, which is the actual harmonic emissions.

Table 7 displays the THD error between the actual and predicted signals, which is calculated as in Eq. (9).

There is no difference between the simulated and predicted THD. This is due to the high accuracy of the proposed MLRA model. When a pure sinusoidal voltage signal is applied to the expert ANNs system for 800 W/m^2 and 1000 W/m^2 solar irradiance values, respectively, the predicted signals show excellent agreement with that of the simulated system connected to an ideal power source, as in Cases 2 and 4, which reflect the true harmonic distortion of the system under estimation as demonstrated in Fig. 14 and Fig. 15.

The FFT solution for the two signals was performed in MATLAB, and the results highlight the accuracy of the MLRA model in terms of the individual significant harmonic components with zero error. The Robust MLRA system

TABLE 5. The progression of MLRA training among various models.

No.	Fav.	Model No.	Model Type	Status	RMSE Valid.	MSE Valid.	R^2 Valid.	MAE Valid.	Prediction Speed (obs/sec)	Training Time (sec)
1	**0**	1	Tree	Trained	0.2450	0.06003	0.958454	0.144103	3150.151	9.7298466
2	**0**	2.1	Linear Regression	Trained	2.479e-13	6.149e-26	1	4.519e-14	3233.530	4.1706618
3	**0**	2.2	Linear Regression	Trained	1.612e-11	2.599e-22	1	2.810e-12	446.6631	5.9433993
4	**1**	**2.3**	**Linear Regression**	**Trained**	**1.184e-13**	**1.402e-26**	**1**	**2.854e-14**	**1156.495**	**6.9521883**
5	**0**	2.5	Tree	Trained	0.245025	0.060037	0.958454	0.144103	2919.600	2.3538579
6	**0**	2.6	Tree	Trained	0.366203	0.13410	0.907200	0.245599	3747.910	4.3014908
7	**0**	2.7	Tree	Trained	0.810514	0.656933	0.545407	0.684148	3684.769	1.3351303
8	**0**	2.8	SVM	Trained	0.078400	0.006146	0.995746	0.071569	1780.355	5.5768334
9	**0**	2.9	SVM	Trained	0.099290	0.009858	0.993177	0.078498	2882.038	3.8986099
10	**0**	2.1	SVM	Trained	0.165196	0.027290	0.981115	0.106151	2501.233	3.4943604
11	**0**	2.11	SVM	Trained	0.804567	0.647328	0.552054	0.496137	3126.716	3.004708
12	**0**	2.12	SVM	Trained	0.317966	0.101102	0.930034	0.179799	2489.124	5.2340688
13	**0**	2.13	SVM	Trained	0.196887	0.038764	0.973175	0.13462	1578.430	4.8202256
14	**0**	2.14	Ensemble	Trained	3.540666	12.53631	7.675018	3.53525	927.2787	5.2754198
15	**0**	2.15	Ensemble	Trained	0.256983	0.066040	0.954300	0.14260	921.015	4.9107442
16	**0**	2.16	Gaussian	Trained	0.000399	1.594e-07	0.999999	0.000243	3092.059	6.7028305
17	**0**	2.17	Gaussian	Trained	0.000399	1.597e-07	0.999999	0.000243	3752.839	1.3715976
18	**0**	2.18	Gaussian	Trained	0.124758	0.015564	0.989229	0.06987	2700.493	2.6984924
19	**0**	2.19	Gaussian	Trained	0.000399	1.594e-07	0.999999	0.000243	2986.785	2.9533971
20	**0**	2.2	NN	Trained	0.224165	0.05024	0.965227	0.047821	2946.438	7.2796473
21	**0**	2.21	NN	Trained	0.350638	0.122947	0.914921	0.118882	2874.024	6.7967107
22	**0**	2.22	NN	Trained	0.629131	0.39580	0.726105	0.247505	3488.163	10.0920468
23	**0**	2.23	NN	Trained	0.558627	0.312064	0.784053	0.100939	3403.039	10.5300595
24	**0**	2.24	NN	Trained	0.096965	0.009402	0.993493	0.026461	3532.095	12.3229052
25	**0**	2.25	Kernel	Trained	0.718825	0.516710	0.642441	0.428202	1986.463	12.076443
26	**0**	2.26	Kernel	Trained	0.753084	0.567139	0.607546	0.510134	3088.205	10.299545

TABLE 6. Robust linear regression training parameters.

RMSE (Validation)	$1.184e^{-13}$
R-squared (Validation)	1.00
MSE (Validation)	$1.402e^{-2}6$
MAE (Validation)	$2.854e^{-14}$
Prediction speed	1156.495
Training Time (hh:mm: ss: ^{oo})	00:00:6.95

TABLE 7. THD error% between the actual and predicted signals.

Solar Irradiance (W/m^2)	Simulated PCC voltage THD %	Simulated PCC voltage THD %	% Error
1000	16.4%	16.4%	0%
800	19.1%	19.1%	0%

computational complexity with large numbers of inputs is a crucial factor that must be considered during the training and prediction stages. It is well understood that the greater the number of inputs for a given size of data, the greater the computational time required for convergence. But in the proposed algorithm the training and forecasting processes took about 6.9 seconds, in the training process which yields in fast response in online harmonic identification this represents a computational burden. Moreover, enough samples obtained a high accuracy and zero prediction error.

1) F-TEST

The standard rule of thumb of regression is that if $F > 2.5$, the null hypothesis can be rejected. We can conclude that at least

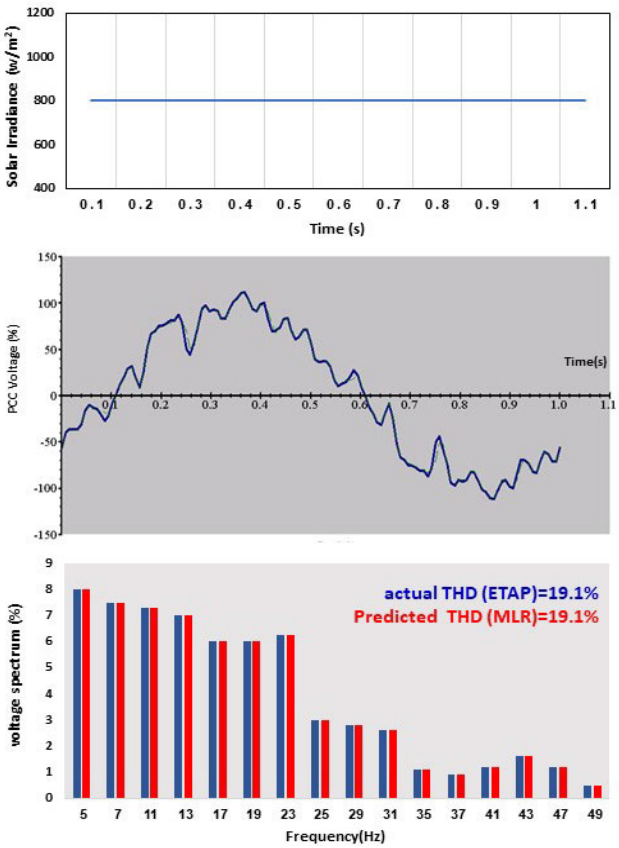

FIGURE 14. The proposed method's performance at 800 W/m^2.

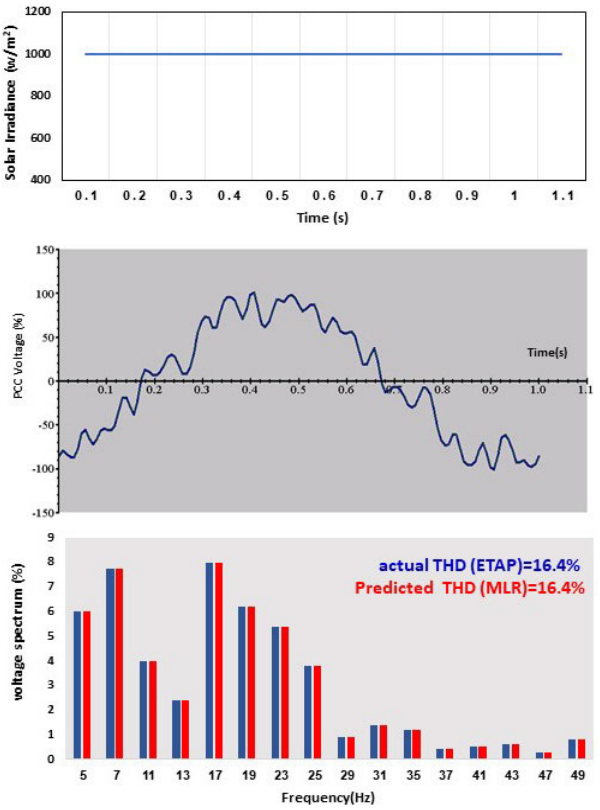

FIGURE 15. The proposed method's performance at 1000 W/m^2.

one parameter value is nonzero. Applying Equation (26) to calculate the F-test [67, it can be noticed that F = 0 for THD prediction by Robust MLRA model.

2) T-TEST

A "good" t-statistic or t-value in regression is one that is significantly higher in absolute value than the critical value from the t-distribution for a given significance level, which is typically around two or -2 for a 95% confidence level. This shows that the coefficient is statistically significant. When taking samples, there is a good chance that the t-value will be zero. It makes sense — if the null hypothesis is correct, the t-value should be zero because there is no signal. However, the further the t-value is from zero, the less likely we are to obtain it. By applying Eq. (27) to the study, for THD prediction, t-Test equal zero. Table 8 depicts the Robust MLRA performance during the Test phase:

TABLE 8. Robust linear regression test parameters.

RMSE (Validation)	7.2637e-15
R-squared (Validation)	1.00
MSE (Validation)	5.2761e-29
MAE (Validation)	3.7127e-15
F-Test	0
t-Test	0

V. VALIDATION

In this section, an extensive comparative analysis is included to validate the use of AI techniques. Two scenarios are used as follows:

1. IEEE 9-bus, microgrid system applying ANFIS, ANNs, MLRA.
2. IEEE 34-bus system applying ANNs, MLRA.

The results of the two scenarios will be demonstrated as in the following:

A. SCENARIO 1: IEEE 9-BUS, MICROGRID SYSTEM APPLYING ANFIS, ANNs, MLRA

The comparison between ANNs, ANFIS and MLRA using two systems, the first one is IEEE 9-bus microgrid include training and test phase as shown in Table 9. The results of applying the three models will be demonstrated. In this section, the three models; ANNs, ANFIS and MLR were applied to the IEEE 9-bus microgrid system to validate the MLRA model. The system was as shown in Fig. 16. The obtained results of each model based on its algorithm were compared in the training and test process.

The comparison criteria will depend on the road's performance in predicting the total harmonic distortion coefficient. In this case, the performance is evaluated according to RMSE, R^2, MSE, and MAE as well as equations (1) and (2), taking

TABLE 9. Comparison between ANNs, ANFIS and MLR in training phase.

MODEL	ANNs	ANFIS	MLR
RMSE (Validation)	0.97588	5.278 e-05	0.095
R-squared (Validation)	0.99254	0.9857	1.00
MSE (Validation)	0.95234	2.7e-11	0.009035
MAE (Validation)		0.082377	0.048734
Prediction speed	Terribly slow	slow	1100 obs/s
Training Time (hh:mm:ss:^{ms})	02:45:54	00:30:20	00:00:3:58

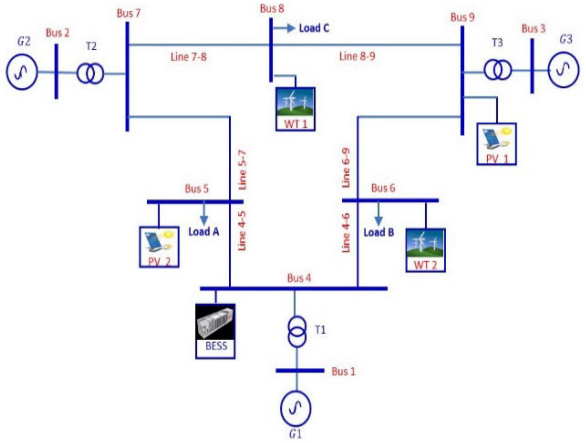

FIGURE 16. IEEE 9-BUS standardtest network.

into account the time consumed in training and testing the model.

1) TRAINING PHASE

A comparison of the three techniques used to forecast harmonics in the 9-bus IEEE microgrid system during the training phase is presented in Table 9 below. Moreover, Fig. 17 depicts the prediction response of each model in training phase.

The prediction response of each model in training phase.

From the obtained results in Table 9, and Fig 17, it can be noticed that there is a small difference between RMSE value and MSE for ANNs and ANFIS results. However, MLR has good results among the three models. Moreover, there is a considerable time consumed with the MLR technique. *It is noticed From Table 9 that:*

1. The MLR has reached the global optimal solution in considerable low time.
2. The MLR achieved higher value squared error (R^2).
3. The MLR consumes the lowest training time.
4. As a result of remark 2, the prediction speed of MLR is the best one.

2) TEST PHASE

A comparison of the three algorithms used to forecast harmonics in the microgrid system under study during the test stage is illustrated in Table 10 below.

Table 10 summarizes the test results for the three applied techniques that were used to predict the total harmonic

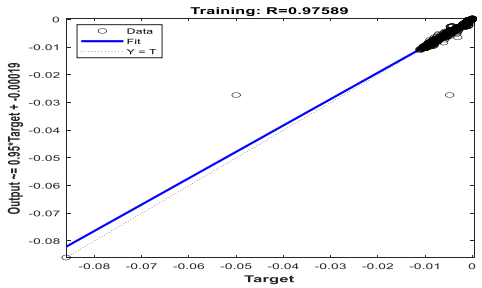

a. ANNs

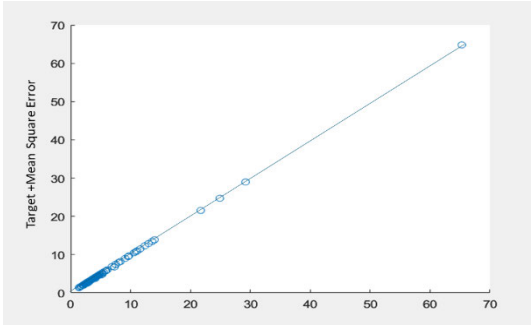

b. ANFIS

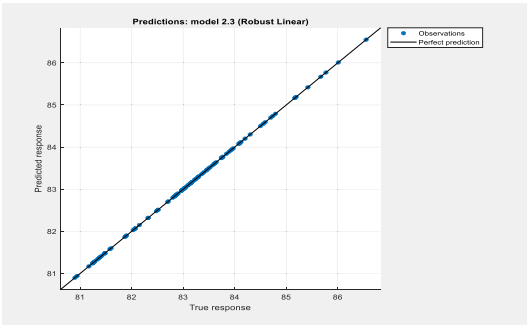

c. MLRA

FIGURE 17. The prediction response of each model in training phase.

TABLE 10. Comparison between ANNs, ANFIs and MLR in the test phase.

MODEL	ANNs	ANFIS	MLR
RMSE (Validation)	0.00088	0.26055	0.47696
R-squared (Validation)	0.95455	0.9544	0.98
MSE (Validation)	7.77e-07	0.06788	0.22749
MAE (Validation)	8.916E-07	0.07790	0.19824

distortion online as a first step to mitigate the harmonics in 9-bus IEEE microgrid system. As Table 10 illustrates:

1. The global optimal solution was found by the MLR in a surprisingly brief time.
2. The MLR had a higher value squared error (R^2).
3. The MLR has the shortest training time requirement.
4. MLR has the fastest prediction speed due to remark 2.

B. SCENARIO 2: IEEE 34-BUS SYSTEM APPLYING ANNs, MLRA

The IEEE 34-bus test feeder with the solar PV-1 system and different harmonic sources presented in [74] is modelled and simulated using Electric Transient Analysis Programme (ETAP) to validate the proposed ANNs-based

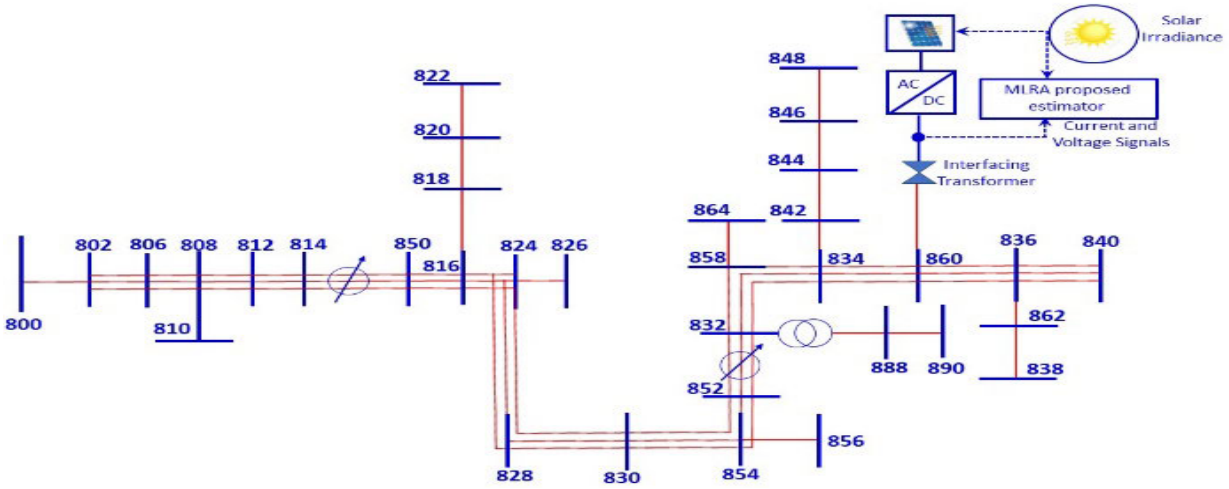

FIGURE 18. The tested IEEE distributed redial 34-BUS feeder.

harmonic distortions estimator. The feeder loading conditions were maintained in accordance with the IEEE Power & Energy Society working group specifications [75]. The Robust MLRA system computational complexity with this section introduces the IEEE 34-bus test feeder and the factors that influenced the decision on the simulated system. Also shown are the simulated harmonic sources. Furthermore, the results are evaluated and presented. Even though it is one of the most frequently used feeders for establishing harmonic prediction and detection solutions, The IEEE 34-bus system is a more complicated distribution system with an extremely lengthy feeder that necessitates the use of voltage regulators to meet ANSI voltage standards. The IEEE 34-bus is only made up of six medium-voltage three-phase buses. in the following, the characteristics of the 34 bus feeders [76]:

1. Various kinds of loads
   - All spot loads connected.
   - delta and Wye connected.
   - A combination of constant current, constant power, and constant impedance.
2. Line Styles
   - Overhead three-phase (a-n, b-n, and c-n).
   - Overhead single-phase (a-n, b-n, and c-n).
3. Voltage Regulators - single-phase wye-connected regulators.
4. Shunt Capacitors.
   - Balanced three-phase.

Because of its length and low loading condition, the IEEE distributed redial 34-bus test feeder depicted in Fig. 18 was employed to connect the harmonic sources that will be emulated in this paper. The solar PV-1 system, as well as the various harmonic sources used, will be connected to the green-highlighted nodes. For each run, each harmonic source will be connected to a different bus, while the solar PV-1 system will remain connected to bus-860 [77]. Because the purpose of this study is to estimate total harmonic distortions in a PE-based application, various harmonic sources are simulated, including 6 and 12 pulse power rectifiers, DC motor, thyristor controlled Reactors (TCR), and static frequency converters (SFC). Based on the field measurements in [46], harmonic current sources are used to model these harmonic sources.

The outcomes were acquired through a methodical allocation of the different harmonic sources among the eighteen viable three-phase nodes found in the green-highlighted buses. The Minitab program Ver-16 will be used in this section to extract the relation among the solar irradiance and the other significant factors. Using the two solar irradiance points (800 and 1000 W/m^2) and the five harmonic sources listed in Table 11, a total of 170 tests were conducted. The suggested MLRA -based harmonic distortions estimator was used to process, save the simulated voltage, and current signals from each run-in order to forecast the harmonic distortions of the solar PV-1 system. The proposed MLRA -based estimator's predicted signals are compared to the harmonic current components listed in Table 11, and as illustrated

TABLE 11. Individual harmonic content of harmonic sources [44].

Harmonic order	3	5	7	9	11	13	15	17	19	21	23	25
6-pulse	0.015	0.22	0.150	-	0.102	0.084	-	0.043	0.034	-	0.006	-
12-pulse	0.002	0.006	0.003	-	0.062	0.045	-	0.001	0.002	-	0.005	-
SFC	-	0.17	0.101	-	0.061	0.044	-	0.038	0.032	-	0.026	0.023
DC motor	0.138	0.051	0.026	0.016	0.011	0.008	0.006	0.004	0.004	0.003	0.003	0.002
TCR	0.012	0.336	0.016	-	0.087	0.012	-	0.045	0.013	-	0.028	-

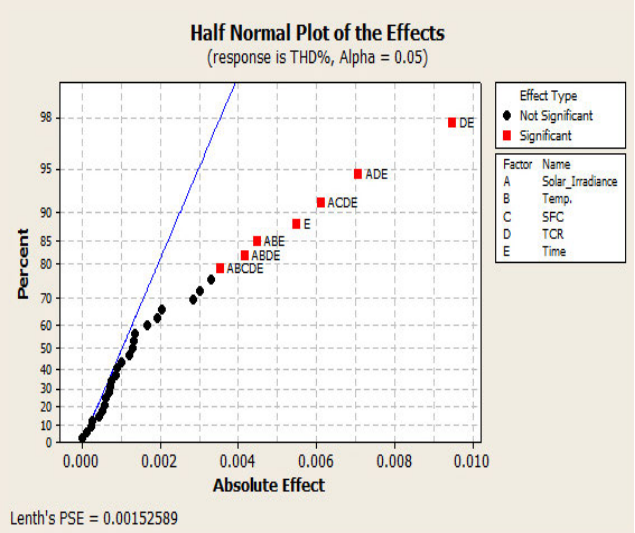

FIGURE 19. The half normal plot of the effects sola irradiance.

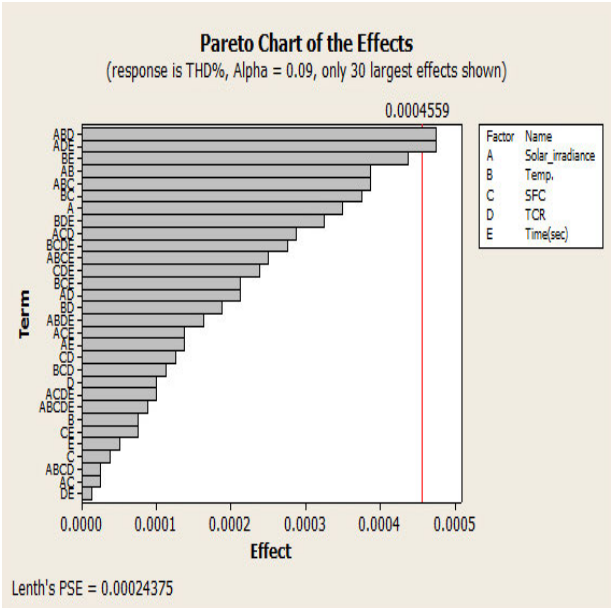

FIGURE 20. Pareto chart of the effects solar irradiance.

in Eq. (8), the error of each corresponding component is computed for every test run. A-phase voltage and current signals were fed into the suggested estimator to minimize computational effort.

The variations at the network level were disregarded because there were no PFC capacitors and the loading conditions stayed constant throughout the simulation. Figure 19 illustrates that solar radiation responds to transformers' TCR more than SFC. Where the power grid networks provide electricity as AC (alternating current), however, for some essential applications, like charging electric vehicles (EVs) and Egypt's monorail transport systems, DC (e.g., 750–1500 volts) is needed for an economical and effective operation [78], [79].

The power network, on the other hand, provides much higher-voltage AC with high harmonic distortion.

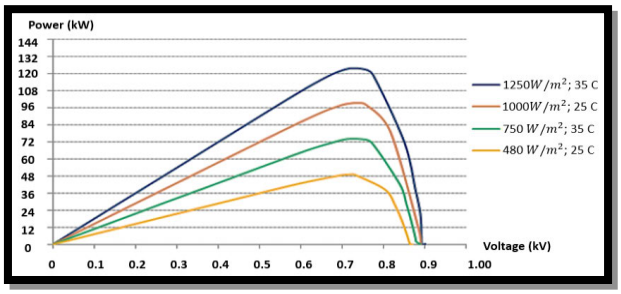

FIGURE 21. P-V characteristics at different radiation and temperatures intensities.

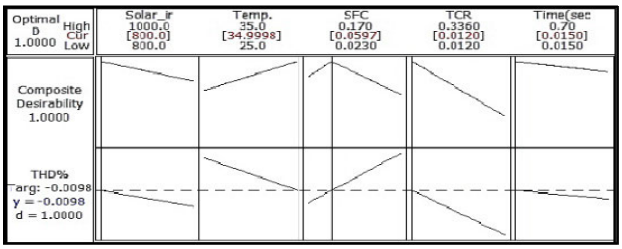

FIGURE 22. The optimal sets of individual harmonic contents of harmonic source.

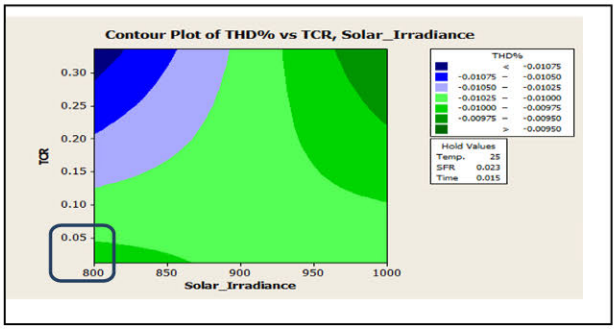

FIGURE 23. The contour plot of THD% vs TCR, affect solar irradiance.

Transformers and rectifiers are, hence, essential converters for network power conversion from AC to DC. For control circuits, rectifiers are useful, particularly thyristors. Fig. 19 illustrates that harmonic distortion responds to TCR with time; this converter is compatible with solar cells that are considered a photovoltaic source (DC current) that operates continuously when exposed to sunlight.

Therefore, the radiation intensity can be expressed as in Eq. (29), which directly correlates with the current quantity generated according to time as:

$$I_g = I_{SCR}\frac{G}{G_R}[1 + \alpha_T(T_C - T_{CR})] \tag{29}$$

where G is the irradiance value in W/m^2 and I_{SCR} is the short circuit current at the reference solar radiation G_R and the reference cell temperature T_{CR}, and α_T is a constant temperature coefficient (0.0017 A/K in case of silicon solar cell) of the photo current.

Fig. 20 emphasizes temperature effects on TCR efficiency when used to rectify the current of solar irradiance. Therefore, the study includes two levels of temperature [25 – 35 °C] and

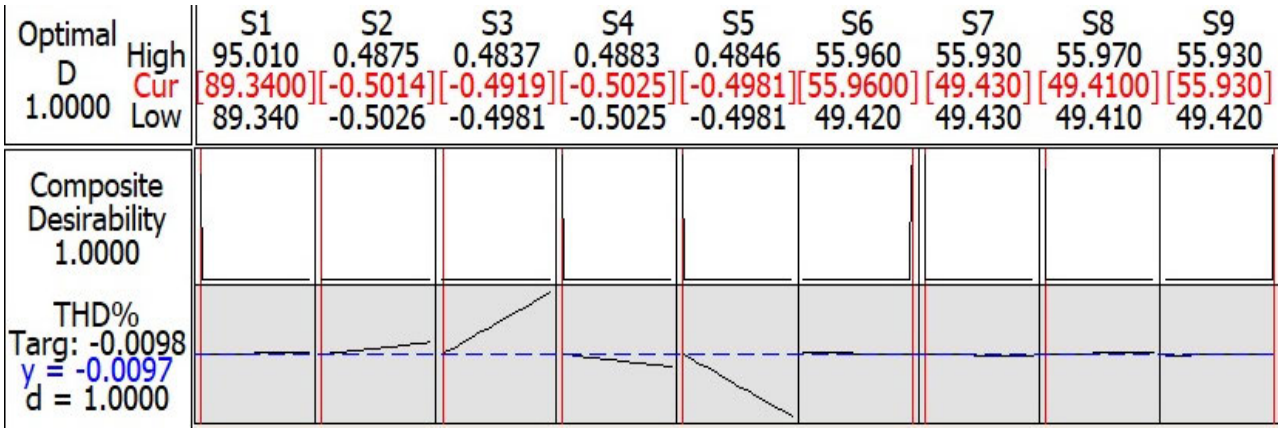

FIGURE 24. The suggested voltage FED to the grid to eliminate the distortion.

TABLE 12. Comparison between ANNs and LRA in training phase.

MODEL	ANNs	MLRA
RMSE (Validation)	0.97588	0.184e-13
R-squared (Validation)	0.99254	1.00
MSE (Validation)	0.95234	1.402e-26
MAE (Validation)		2.855e-14
Prediction speed	Too slow	1200 obs/s
Training Time (hh:mm: ss: ^{oo})	03:11:54	00:00:6:9

Figure 21 illustrates that high efficiency can be gained from 25 °C and economically present between 750-1000 kW/m^2.

According to Table 12 and Figure 22 in case of economic gain eight hundred kW/m^2 prefer to set the temperature at 35, and individual harmonic TCR at 0.012, SFC at 0.0597, which picked at time 0.015 after 0.1. Figure 23 illustrates that if we set TCR at 0.012 and the temperature becomes twenty-five °C, then the SFC values must maintain the distortion at a low level and be found to be 0.023 Before 0.015 of a second has passed. This challenge emphasizes that machine learning that distinguishes with quick response is preferred. To reduce the total THD% maintain the fueled voltage by the converters and rectifiers set at minimum values except buses 6, 9, 12, and 15 as suggested in Figure 24 to gain minimum distortion -0.0097.

1) TRAINING PHASE

The harmonic contents of current signal that resulted from the developed harmonic sources were simulated using the base values listed. Furthermore, as discussed in Section IV, the sampling settings for the simulated signals were set, and by using ETAP the total harmonic distortions can be obtained. A comparison between the two techniques used to forecast harmonics in the IEEE 34-bus microgrid system during the training phase is presented in Table 12. Moreover, Fig. 25 depicts the prediction response of each model in the training phase. Also, there is a small difference between RMSE value and MSE for ANNs and ANFIS results. However, MLRA has satisfactory results among the three models. Moreover, there is a considerable time consumed with the MLRA technique. It is noticed from Table 12, the MLRA has reached the optimal global solution in considerable low time. The MLRA achieved higher value squared error (R^2) and consumed the lowest training time compared with ANNs and ANFIS techniques.

TABLE 13. Comparison between ANNs and MLRA in test phase.

MODEL	ANNs	MLRA
RMSE (Validation)	0.00088	7.2637e-15
R-squared (Validation)	0.95455	1
MSE (Validation)	7.77e-07	5.276e-29
MAE (Validation)	8.916E-07	3.7127e-15

2) TEST PHASE

A comparison between the three algorithms applied to forecast harmonics in the microgrid under study during the test stage is illustrated in Table 13 below. Moreover, Fig. 25 depicts the prediction response of each model in the test stage. This figure shows the predicted THD values in the test case for the three applied techniques in this research. The three methods gave close values in the case of training, as $R^2 = 0.99$, 1 in the three methods: ANNs and MLRA, respectively. However, the time taken for training in the case of MLRA is much shorter, which gives MLRA priority in the three methods for predicting the coefficient of the Harmonic distortion.

Table 13 summarizes the test results for the three applied techniques that were predicted the total harmonic distortion as a first step to mitigate the harmonics in 34-bus IEEE system. As illustrated in Table 13, the global optimal solution was found by the MLRA in a surprisingly short time. The MLRA had a higher value squared error (R^2). The MLRA has the shortest training time requirement. MLRA has the fastest prediction speed. Figure 26 depicts the predicted THD values in the test phase for the three under study techniques in this research. It is clear that the MLRA leads to the best accurate prediction compared with other techniques with the squared error index of $R^2 = 0.98$.

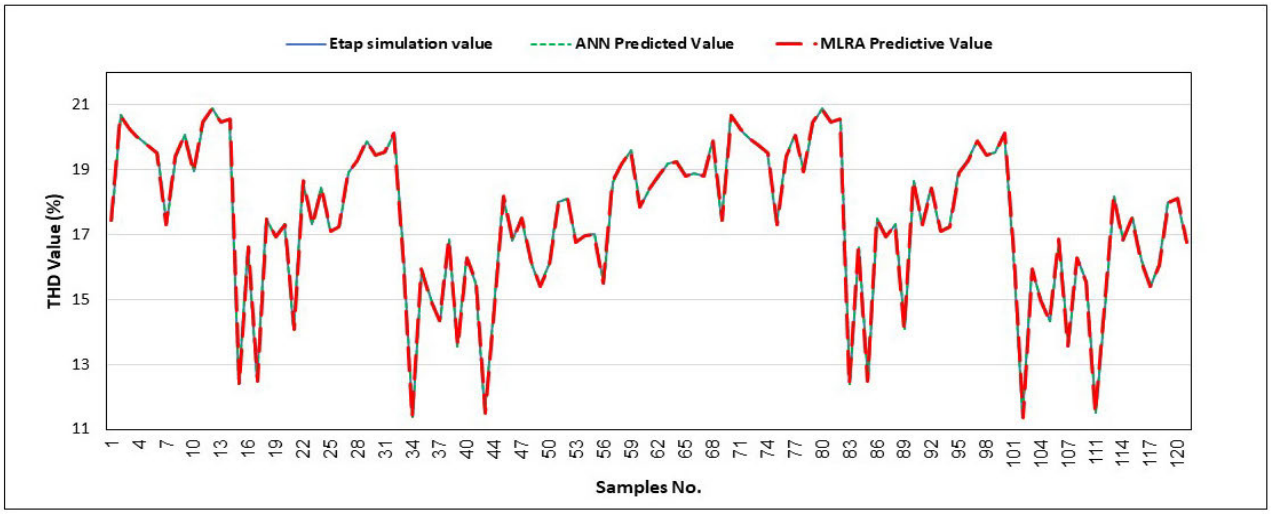

FIGURE 25. Comparison between the actual THD value and predictive THD using the two models under study during training phase.

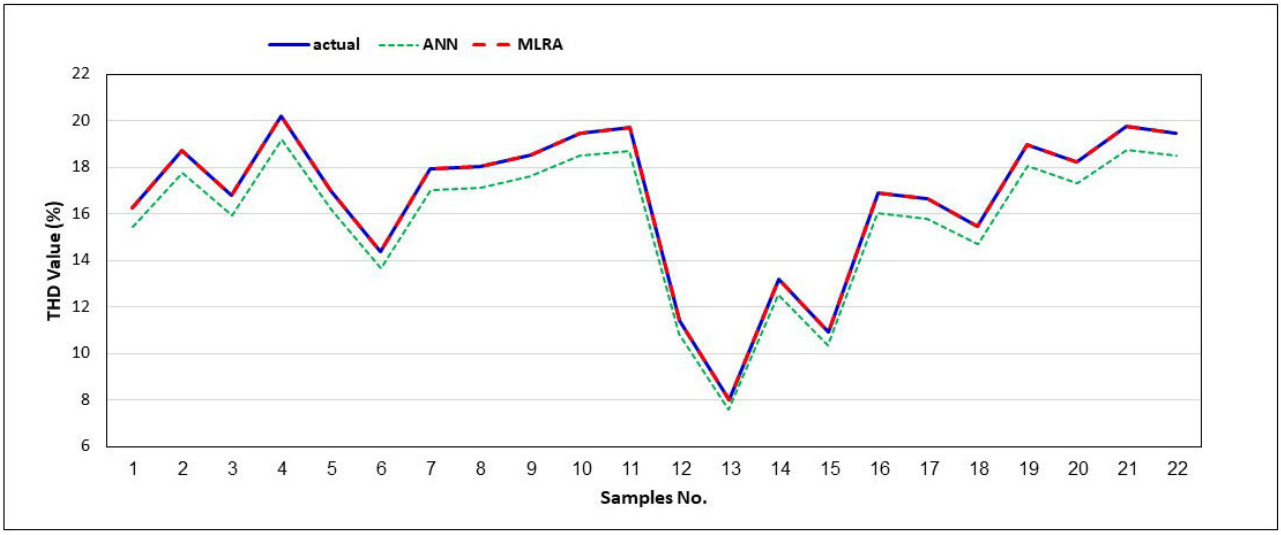

FIGURE 26. Comparison between the actual THD value and predictive THD using the two models under study during test phase.

VI. CONCLUSION

This paper investigates an approach for harmonic detection in microgrid using artificial intelligent techniques. The multiple sources of harmonics in the tested microgrid are considered as the uncertain PV and Wind systems. To capture the accurate levels of harmonic distortions, a linear regression and location-specific data were developed. The training process is carried out by machine learning regression to achieve high performance of the harmonic detection and preserve the estimation error at the lowest levels. In this study, the total harmonic distortion of a 34-bus IEEE microgrid was predicted using two intelligent based methods called machine linear regression and artificial neural networks. The MLRA based detection leads to more accurate THD estimation compared with those obtained by ANNs. Furthermore, when it comes to predicting the THD values of an oriented strand board, it performs better, faster, and requires less time to train than ANNs. Four cases are carried out with two profiles of the harmonic sources.

The future of this study can be considered to model different types of harmonic sources resulted from the inverters associated with renewable energies. Also, the advanced models based on signal processing to alleviate the problems of data uncertainty.

FUTURE WORK

The future of this study can be considered to model different types of harmonic sources resulting from the inverters associated with renewable energies. Also, advanced models based on signal processing alleviate the problems of data uncertainty. The research idea is expected to lead to an increase in the percentage of microgrid systems to 3.87%. This is due to the fact that the size of the distortion and the resulting loss to the microgrids won't affect the main network, which

will lower the cost of energy use and support the sustainable expansion of microgrid usage to meet SDG 8 and expect improving in the GDP per capita [4].

ACKNOWLEDGMENT

This work was supported in part by Prince Sattam bin Abdulaziz University (PSAU) as part of funding for its SDG (Sustainable Development Goals) Roadmap Research Funding Programme project number PSAU-2023-SDG-22.

CONTRIBUTION

Ahmed M. Abed: Writing – review & editing, Writing – original draft, Validation, Software, Methodology, Resources, Data Curation, Funding acquisition, Formal analysis, Supervision. **Ragab A. El-Sehiemy:** Writing – original draft, Validation, Software, Formal analysis, Conceptualization, Supervision. **Bachir Bentouati:** Writing – original draft, Validation, Software, Methodology, Formal analysis, Conceptualization. **Hasnaa M. El-Arwash:** Writing – original draft, Validation, Software, Methodology, Formal analysis, Investigation, Resources, Conceptualization, Supervision.

CONFLICTS OF INTEREST

There is no conflict of interest among authors.

DATA AVILABILITY STATEMENT

Data and code will be available upon requests.

REFERENCES

[1] M. Rezkallah, A. Chandra, A. Hamadi, H. Ibrahim, and M. Ghandour, "Power quality in smart grids," in *Pathways to a Smarter Power System*. Academic, 2019, pp. 225–245.

[2] *IEEE Recommended Practices and Requirements for Harmonic Control in Electrical Power Systems*, New York, NY, USA, 1993, doi: 10.1109/ieeestd.1993.114370.

[3] A. M. Abed and A. Alarjani, "The neural network classifier works efficiently on searching in DQN using the autonomous Internet of Things hybridized by the metaheuristic techniques to reduce the EVs' service scheduling time," *Energies*, vol. 15, no. 19, p. 6992, Sep. 2022, doi: 10.3390/en15196992.

[4] L. F. Seddek and A. M. Abed, "Discuss the effect of the third organizational efficiency theory on society and economic growth via depravity axes frustration by a non-linear model (depravity aspects benefits)," *Int. J. Membrane Sci. Technol.*, vol. 10, no. 1, pp. 1252–1271, Oct. 2023, doi: 10.15379/ijmst.v10i1.2837.

[5] S. Ahmad, H. Mubarak, U. K. Jhuma, T. Ahmed, S. Mekhilef, and H. Mokhlis, "Point of common coupling voltage modulated direct power control of grid-tied photovoltaic inverter for AC microgrid application," *Int. Trans. Electr. Energy Syst.*, vol. 2023, pp. 1–22, May 2023, doi: 10.1155/2023/3641907.

[6] A. M. Abed, L. F. Seddek, and S. Elattar, "Building a digital twin simulator checking the effectiveness of TEG-ICE integration in reducing fuel consumption using spatiotemporal thermal filming handled by neural network technique," *Processes*, vol. 10, no. 12, p. 2701, Dec. 2022, doi: 10.3390/pr10122701.

[7] J. H. R. Enslin and P. J. M. Heskes, "Harmonic interaction between a large number of distributed power inverters and the distribution network," *IEEE Trans. Power Electron.*, vol. 19, no. 6, pp. 1586–1593, Nov. 2004, doi: 10.1109/TPEL.2004.836615.

[8] J. Mazumdar, R. G. Harley, F. C. Lambert, G. K. Venayagamoorthy, and M. L. Page, "Intelligent tool for determining the true Harmonic-Current contribution of a customer in a power distribution network," *IEEE Trans. Ind. Appl.*, vol. 44, no. 5, pp. 1477–1485, Sep. 2008, doi: 10.1109/TIA.2008.2002213.

[9] W. Xu and Y. Liu, "A method for determining customer and utility harmonic contributions at the point of common coupling," *IEEE Trans. Power Del.*, vol. 15, no. 2, pp. 804–811, Apr. 2000, doi: 10.1109/61.853023.

[10] W.-M. Lin, T.-S. Zhan, and M.-T. Tsay, "Multiple-frequency three-phase load flow for harmonic analysis," *IEEE Trans. Power Syst.*, vol. 19, no. 2, pp. 897–904, May 2004, doi: 10.1109/TPWRS.2004.825906.

[11] C. Li, W. Xu, and T. Tayjasanant, "A 'critical impedance'-based method for identifying harmonic sources," *IEEE Trans. Power Del.*, vol. 19, no. 2, pp. 671–678, Apr. 2004, doi: 10.1109/TPWRD.2004.825302.

[12] R. A. S. Fernandes, M. Oleskovicz, and I. N. da Silva, "Harmonic source location and identification in radial distribution feeders: An approach based on particle swarm optimization algorithm," *IEEE Trans. Ind. Informat.*, vol. 18, no. 5, pp. 3171–3179, May 2022, doi: 10.1109/TII.2021.3108681.

[13] F. Ruiz-Rodriguez, J. Hernandez, and F. Jurado, "Harmonic modelling of PV systems for probabilistic harmonic load flow studies," *Int. J. Circuit Theory Appl.*, vol. 43, no. 11, pp. 1541–1565, Sep. 2014, doi: 10.1002/cta.2021.

[14] F. J. Ruiz-Rodriguez, J. C. Hernandez, and F. Jurado, "Iterative harmonic load flow by using the point-estimate method and complex affine arithmetic for radial distribution systems with photovoltaic uncertainties," *Int. J. Electr. Power Energy Syst.*, vol. 118, Jun. 2020, Art. no. 105765, doi: 10.1016/j.ijepes.2019.105765.

[15] J. C. Hernandez, F. J. Ruiz-Rodriguez, F. Jurado, and F. Sanchez-Sutil, "Tracing harmonic distortion and voltage unbalance in secondary radial distribution networks with photovoltaic uncertainties by an iterative multiphase harmonic load flow," *Electric Power Syst. Res.*, vol. 185, Aug. 2020, Art. no. 106342, doi: 10.1016/j.epsr.2020.106342.

[16] A. F. Zobaa, "Voltage harmonic reduction for randomly time-varying source characteristics and voltage harmonics," *IEEE Trans. Power Del.*, vol. 21, no. 2, pp. 816–822, Apr. 2006, doi: 10.1109/TPWRD.2005.864043.

[17] R. Cisneros-Magaña, A. Medina-Rios, C. R. Fuerte-Esquivel, and J. Segundo-Ramírez, "Harmonic state estimation based on discrete exponential expansion, singular value decomposition and a variable measurement model," *Energy*, vol. 249, Jun. 2022, Art. no. 123712, doi: 10.1016/j.energy.2022.123712.

[18] R. J. Betancourt, E. Barocio, C. M. Rergis, J. M. González-López, and A. C. Sánchez, "A spatio-temporal processing Padé approach for visualizing harmonic distortion propagation on electrical networks," *Electric Power Syst. Res.*, vol. 203, Feb. 2022, Art. no. 107643, doi: 10.1016/j.epsr.2021.107643.

[19] J. Liang, S. Zhang, Y. Ren, and Y. Cheng, "Harmonics current detection in three-phase circuit using neural network," *J. Phys., Conf.*, vol. 2242, no. 1, Apr. 2022, Art. no. 012043, doi: 10.1088/1742-6596/2242/1/012043.

[20] T. G. Manjunath, A. C. Vikramathithan, and H. Girish, "Analysis of total harmonic distortion and implementation of inverter fault diagnosis using artificial neural network," *J. Phys., Conf.*, vol. 2161, no. 1, Jan. 2022, Art. no. 012060, doi: 10.1088/1742-6596/2161/1/012060.

[21] T. A. Jumani, M. W. Mustafa, N. N. Hamadneh, S. H. Atawneh, M. M. Rasid, N. H. Mirjat, M. A. Bhayo, and I. Khan, "Computational intelligence-based optimization methods for power quality and dynamic response enhancement of AC microgrids," *Energies*, vol. 13, no. 16, p. 4063, Aug. 2020, doi: 10.3390/en13164063.

[22] A. Eslami, M. Negnevitsky, E. Franklin, and S. Lyden, "Review of AI applications in harmonic analysis in power systems," *Renew. Sustain. Energy Rev.*, vol. 154, Feb. 2022, Art. no. 111897, doi: 10.1016/j.rser.2021.111897.

[23] A. Taghvaie, T. Warnakulasuriya, D. Kumar, F. Zare, R. Sharma, and D. M. Vilathgamuwa, "A comprehensive review of harmonic issues and estimation techniques in power system networks based on traditional and artificial intelligence/machine learning," *IEEE Access*, vol. 11, pp. 31417–31442, 2023, doi: 10.1109/ACCESS.2023.3260768.

[24] A. M. Shaheen, R. A. El-Sehiemy, and S. M. Farrag, "Adequate planning of shunt power capacitors involving transformer capacity release benefit," *IEEE Syst. J.*, vol. 12, no. 1, pp. 373–382, Mar. 2018, doi: 10.1109/JSYST.2015.2491966.

[25] R. M. Rizk-Allah, H. M. A. Mageed, R. A. El-Sehiemy, S. H. E. A. Aleem, and A. El Shahat, "A new sine cosine optimization algorithm for solving combined non-convex economic and emission power dispatch problems," *Int. J. Energy Convers. (IRECON)*, vol. 5, no. 6, p. 180, Nov. 2017, doi: 10.15866/irecon.v5i6.14291.

[26] J. Choudhary, D. K. Singh, S. N. Verma, and K. Ahmad, "Artificial intelligence based control of a shunt active power filter," *Proc. Comput. Sci.*, vol. 92, pp. 273–281, Jan. 2016, doi: 10.1016/j.procs.2016.07.356.

[27] L. L. Lai, W. L. Chan, C. T. Tse, and A. T. P. So, "Real-time frequency and harmonic evaluation using artificial neural networks," *IEEE Trans. Power Del.*, vol. 14, no. 1, pp. 52–59, Jan. 1999, doi: 10.1109/61.736681.
[28] H. C. Lin, "Intelligent neural network-based fast power system harmonic detection," *IEEE Trans. Ind. Electron.*, vol. 54, no. 1, pp. 43–52, Feb. 2007, doi: 10.1109/TIE.2006.888685.
[29] M. N. M. Salleh, N. Talpur, and K. Hussain, "Adaptive neuro-fuzzy inference system: Overview, strengths, limitations, and solutions," in *Proc. Int. Conf. Data Mining Big Data*, (Lecture Notes in Computer Science), 2017, pp. 527–535, doi: 10.1007/978-3-319-61845-6_52.
[30] S. Vlahinic, D. Brnobic, and D. Vucetic, "Measurement and analysis of harmonic distortion in power distribution systems," *Electric Power Syst. Res.*, vol. 79, no. 7, pp. 1121–1126, Jul. 2009, doi: 10.1016/j.epsr.2009.02.004.
[31] P. S. Wright, A. E. Christensen, P. N. Davis, and T. Lippert, "Multiple-site amplitude and phase measurements of harmonics for analysis of harmonic propagation on Bornholm island," *IEEE Trans. Instrum. Meas.*, vol. 66, no. 6, pp. 1176–1183, Jun. 2017, doi: 10.1109/TIM.2017.2660019.
[32] Y. Wang, J. Yong, Y. Sun, W. Xu, and D. Wong, "Characteristics of harmonic distortions in residential distribution systems," *IEEE Trans. Power Del.*, vol. 32, no. 3, pp. 1495–1504, Jun. 2017, doi: 10.1109/TPWRD.2016.2606431.
[33] C. Ge, R. A. D. Oliveira, I. Y. H. Gu, and M. H. J. Bollen, "Unsupervised deep learning and analysis of harmonic variation patterns using big data from multiple locations," *Electric Power Syst. Res.*, vol. 194, May 2021, Art. no. 107042, doi: 10.1016/j.epsr.2021.107042.
[34] H. M. El-Arwash, A. M. Azmy, and E. M. Rashad, "Online harmonic simulation and evaluation in electric power distribution systems," in *Proc. 17th Int. Middle East Power Syst. Conf.* Egypt: Mansoura Univ., Dec. 2015, pp. 1093–1100. [Online]. Available: https://engfac.mans.edu.eg/images/files/Final-Conference-Program-7-12-2015.pdf
[35] J. Mazumdar and R. G. Harley, "Recurrent neural networks trained with backpropagation through time algorithm to estimate nonlinear load harmonic currents," *IEEE Trans. Ind. Electron.*, vol. 55, no. 9, pp. 3484–3491, Sep. 2008, doi: 10.1109/TIE.2008.925315.
[36] J. Mazumdar and R. G. Harley, "Utilization of echo state networks for differentiating source and nonlinear load harmonics in the utility network," *IEEE Trans. Power Electron.*, vol. 23, no. 6, pp. 2738–2745, Nov. 2008, doi: 10.1109/TPEL.2008.2005097.
[37] C. F. Nascimento, A. A. Oliveira, A. Goedtel, and A. B. Dietrich, "Harmonic distortion monitoring for nonlinear loads using neural-network-method," *Appl. Soft Comput.*, vol. 13, no. 1, pp. 475–482, Jan. 2013, doi: 10.1016/j.asoc.2012.08.043.
[38] D. Maulud and A. M. Abdulazeez, "A review on linear regression comprehensive in machine learning," *J. Appl. Sci. Technol. Trends*, vol. 1, no. 2, pp. 140–147, Dec. 2020, doi: 10.38094/jastt1457.
[39] Z. Cui and G. Gong, "The effect of machine learning regression algorithms and sample size on individualized behavioral prediction with functional connectivity features," *NeuroImage*, vol. 178, pp. 622–637, Sep. 2018, doi: 10.1016/j.neuroimage.2018.06.001.
[40] R. Trinchero and F. Canavero, "Machine learning regression techniques for the modeling of complex systems: An overview," *IEEE Electromagn. Compat. Mag.*, vol. 10, no. 4, pp. 71–79, May 2021, doi: 10.1109/MEMC.2021.9705310.
[41] M. Maabreh and G. Almasabha, "Machine learning regression algorithms for shear strength prediction of SFRC-DBs: Performance evaluation and comparisons," *Arabian J. Sci. Eng.*, vol. 49, no. 4, pp. 4711–4727, Aug. 2023, doi: 10.1007/s13369-023-08176-y.
[42] J. Wu, C. Liu, W. Cui, and Y. Zhang, "Personalized collaborative filtering recommendation algorithm based on linear regression," in *Proc. IEEE Int. Conf. Power Data Sci. (ICPDS)*, Nov. 2019, pp. 139–142, doi: 10.1109/ICPDS47662.2019.9017166.
[43] A. M. Abdulazeez, B. W. Salim, D. Q. Zeebaree, and D. Doghramachi, "Comparison of VPN protocols at network layer focusing on wire guard protocol," *Int. J. Interact. Mobile Technol. (iJIM)*, vol. 14, no. 18, p. 157, Nov. 2020, doi: 10.3991/ijim.v14i18.16507.
[44] H. Roopa and T. Asha, "A linear model based on principal component analysis for disease prediction," *IEEE Access*, vol. 7, pp. 105314–105318, 2019, doi: 10.1109/ACCESS.2019.2931956.
[45] G. A. F. Seber and A. J. Lee, *Linear Regression Analysis* (Wiley Series in Probability and Statistics), Jan. 2003, doi: 10.1002/9780471722199.
[46] D. C. Montgomery, E. A. Peck, and G. G. Vining, *Introduction to Linear Regression Analysis*. Hoboken, NJ, USA: Wiley, 2021.
[47] S. K. Jain and S. N. Singh, "Fast harmonic estimation of stationary and time-varying signals using EA-AWNN," *IEEE Trans. Instrum. Meas.*, vol. 62, no. 2, pp. 335–343, Feb. 2013, doi: 10.1109/TIM.2012.2217637.
[48] M. Žnidarec, Z. Klaic, D. Sljivac, and B. Dumnic, "Harmonic distortion prediction model of a grid-tie photovoltaic inverter using an artificial neural network," *Energies*, vol. 12, no. 5, p. 790, Feb. 2019, doi: 10.3390/en12050790.
[49] A. Chidurala, T. Kumar Saha, and N. Mithulananthan, "Harmonic impact of high penetration photovoltaic system on unbalanced distribution networks—Learning from an urban photovoltaic network," *IET Renew. Power Gener.*, vol. 10, no. 4, pp. 485–494, Apr. 2016, doi: 10.1049/iet-rpg.2015.0188.
[50] A. Fekik, H. Denoun, N. Benamrouche, N. Benyahia, M. Zaouia, and S. Haddad, "Comparative study of PI and FUZZY DC-voltage control for voltage oriented control-PWM rectifier," in *Proc. 14th Int. Conf. Circuits, Syst., Electron., Control Signal Process.*, 2015, pp. 1–7.
[51] C. Larose, R. Gagnon, P. Prud'Homme, M. Fecteau, and M. Asmine, "Type-III wind power plant harmonic emissions: Field measurements and aggregation guidelines for adequate representation of harmonics," *IEEE Trans. Sustain. Energy*, vol. 4, no. 3, pp. 797–804, Jul. 2013, doi: 10.1109/TSTE.2013.2252209.
[52] H. M. El-Arwash, A. M. Azmy, and E. M. Rashad, "Optimal harmonics compensation in a sea water desalination plant," *Revista de Tehnologii Neconventionale*, vol. 19, no. 4, p. 31, 2015.
[53] S. Kar, S. Das, and P. K. Ghosh, "Applications of neuro fuzzy systems: A brief review and future outline," *Appl. Soft Comput.*, vol. 15, pp. 243–259, Feb. 2014, doi: 10.1016/j.asoc.2013.10.014.
[54] M. Panella, "A hierarchical procedure for the synthesis of ANFIS networks," *Adv. Fuzzy Syst.*, vol. 2012, pp. 1–12, Jan. 2012, doi: 10.1155/2012/491237.
[55] H. A. Zamani, S. Rafiee-Taghanaki, M. Karimi, M. Arabloo, and A. Dadashi, "Implementing ANFIS for prediction of reservoir oil solution gas-oil ratio," *J. Natural Gas Sci. Eng.*, vol. 25, pp. 325–334, Jul. 2015, doi: 10.1016/j.jngse.2015.04.008.
[56] D. Hunter, H. Yu, M. S. PukishIII, J. Kolbusz, and B. M. Wilamowski, "Selection of proper neural network sizes and architectures—A comparative study," *IEEE Trans. Ind. Informat.*, vol. 8, no. 2, pp. 228–240, May 2012, doi: 10.1109/TII.2012.2187914.
[57] J.-S.-R. Jang, "ANFIS: Adaptive-network-based fuzzy inference system," *IEEE Trans. Syst., Man, Cybern.*, vol. 23, no. 3, pp. 665–685, May 1993, doi: 10.1109/21.256541.
[58] V. G. Kinhal, P. Agarwal, and H. O. Gupta, "Performance investigation of neural-network-based unified power-quality conditioner," *IEEE Trans. Power Del.*, vol. 26, no. 1, pp. 431–437, Jan. 2011, doi: 10.1109/TPWRD.2010.2050706.
[59] S. Kavitha, S. Varuna, and R. Ramya, "A comparative analysis on linear regression and support vector regression," in *Proc. Online Int. Conf. Green Eng. Technol. (IC-GET)*, Nov. 2016, pp. 1–5, doi: 10.1109/GET.2016.7916627.
[60] M. S. Acharya, A. Armaan, and A. S. Antony, "A comparison of regression models for prediction of graduate admissions," in *Proc. Int. Conf. Comput. Intell. Data Sci. (ICCIDS)*, Feb. 2019, pp. 1–5, doi: 10.1109/ICCIDS.2019.8862140.
[61] Z. Zhang, Y. Li, L. Li, Z. Li, and S. Liu, "Multiple linear regression for high efficiency video intra coding," in *Proc. IEEE Int. Conf. Acoust., Speech Signal Process. (ICASSP)*, May 2019, pp. 1832–1836, doi: 10.1109/ICASSP.2019.8682358.
[62] M. C. Roziqin, A. Basuki, and T. Harsono, "A comparison of montecarlo linear and dynamic polynomial regression in predicting dengue fever case," in *Proc. Int. Conf. Knowl. Creation Intell. Comput. (KCIC)*, Nov. 2016, pp. 213–218, doi: 10.1109/KCIC.2016.7883649.
[63] A. K. Prasad, M. Ahadi, B. S. Thakur, and S. Roy, "Accurate polynomial chaos expansion for variability analysis using optimal design of experiments," in *IEEE MTT-S Int. Microw. Symp. Dig.*, Aug. 2015, pp. 1–4, doi: 10.1109/NEMO.2015.7415055.
[64] Y. Chen, P. He, W. Chen, and F. Zhao, "A polynomial regression method based on trans-dimensional Markov chain Monte Carlo," in *Proc. IEEE 3rd Adv. Inf. Technol., Electron. Autom. Control Conf. (IAEAC)*, Oct. 2018, pp. 1781–1786, doi: 10.1109/IAEAC.2018.8577769.
[65] G. D. Finlayson, M. Mackiewicz, and A. Hurlbert, "Color correction using root-polynomial regression," *IEEE Trans. Image Process.*, vol. 24, no. 5, pp. 1460–1470, May 2015, doi: 10.1109/TIP.2015.2405336.
[66] N. N. Mohammed and A. M. Abdulazeez, "Evaluation of partitioning around medoids algorithm with various distances on microarray data," in *Proc. IEEE Int. Conf. Internet Things (iThings) IEEE Green Comput. Commun. (GreenCom) IEEE Cyber, Phys. Social Comput. (CPSCom) IEEE Smart Data (SmartData)*, Jun. 2017, pp. 1011–1016, doi: 10.1109/iThings-GreenCom-CPSCom-SmartData.2017.155.

[67] H. Jie and G. Zheng, "Calibration of torque error of permanent magnet synchronous motor base on polynomial linear regression model," in *Proc. 45th Annu. Conf. IEEE Ind. Electron. Soc.*, vol. 1, Oct. 2019, pp. 318–323, doi: 10.1109/IECON.2019.8927537.
[68] H. Niu, Q. Lu, and C. Wang, "Color correction based on histogram matching and polynomial regression for image stitching," in *Proc. IEEE 3rd Int. Conf. Image, Vis. Comput. (ICIVC)*, Jun. 2018, pp. 257–261, doi: 10.1109/ICIVC.2018.8492895.
[69] J. Wolberg, *Data Analysis Using the Method of Least Squares: Extracting the Most Information From Experiments*. Berlin, Germany: Springer, 2006.
[70] J.-H. Xue and D. M. Titterington, "T-tests, F-tests and Otsu's methods for image thresholding," *IEEE Trans. Image Process.*, vol. 20, no. 8, pp. 2392–2396, Aug. 2011, doi: 10.1109/TIP.2011.2114358.
[71] R. Zhang and J. Tian, "Multi-parameter ocean surface wind speed retrieval based on least square method," in *Proc. IEEE Int. Geosci. Remote Sens. Symp. (IGARSS)*, Jul. 2016, pp. 5835–5837, doi: 10.1109/IGARSS.2016.7730524.
[72] H. Chi, "A discussions on the least-square method in the course of error theory and data processing," in *Proc. Int. Conf. Comput. Intell. Commun. Netw. (CICN)*, Dec. 2015, pp. 486–489, doi: 10.1109/CICN.2015.100.
[73] N. V. Sabnis, P. Patil, N. S. Desai, S. Hirikude, S. Ingale, and V. Kulkarni, "Outcome-based education—A case study on project based learning," in *Proc. IEEE 10th Int. Conf. Technol. Educ. (TE)*, Dec. 2019, pp. 248–249, doi: 10.1109/T4E.2019.00058.
[74] X. Wang, F. Blaabjerg, and W. Wu, "Modeling and analysis of harmonic stability in an AC power-electronics-based power system," *IEEE Trans. Power Electron.*, vol. 29, no. 12, pp. 6421–6432, Dec. 2014, doi: 10.1109/TPEL.2014.2306432.
[75] R. Langella, A. Testa, J. Meyer, F. Möller, R. Stiegler, and S. Z. Djokic, "Experimental-based evaluation of PV inverter harmonic and interharmonic distortion due to different operating conditions," *IEEE Trans. Instrum. Meas.*, vol. 65, no. 10, pp. 2221–2233, Oct. 2016, doi: 10.1109/TIM.2016.2554378.
[76] K. Warwick, A. Ekwue, and R. Aggarwal, *Artificial Intelligence Techniques in Power Systems*. Institution of Engineering and Technology, Jun. 1997, doi: 10.1049/pbpo022e.
[77] C.-H. Lin and C.-H. Wang, "Adaptive wavelet networks for power-quality detection and discrimination in a power system," *IEEE Trans. Power Del.*, vol. 21, no. 3, pp. 1106–1113, Jul. 2006, doi: 10.1109/TPWRD.2006.874105.
[78] A. M. El Adawy, "Monorail system as urban sustainable transit in Alexandria," *ERJ. Eng. Res. J.*, vol. 40, no. 4, pp. 349–357, Oct. 2017, doi: 10.21608/erjm.2017.66361.
[79] S. R. Ersoy, J. Terrapon-Pfaff, L. Ribbe, and A. Alami Merrouni, "Water scenarios modelling for renewable energy development in Southern Morocco," *J. Sustain. Develop. Energy, Water Environ. Syst.*, vol. 9, no. 1, p. 11, Mar. 2021, doi: 10.13044/j.sdewes.d8.0335.

AHMED M. ABED received the degree in mechanical engineering, the B.Sc. degree in the industrial and production field, in 2000, the M.Sc. degree from Zagazig University, Egypt (Joint supervision scholarship between Egypt and Germany HTWS Zittau görlitz fachbereich bauwesen hochschule für technik Postfach, Zentralstelle für Arbeitsvermittlung der Bundesanstalt für Arbeit), in 2006, and the Ph.D. degree in Egypt, in 2014. He has a good reputation in this field in more than eight Factories in Industrial 10th of Ramadan City as a consultant. He is an Associate Professor in the IE Department at Zagazig University, AIET, and Prince Sattam bin Abdulaziz University, KSA. He has remarkable public service work as a Treasurer of Engineering Club Syndicate in 10th of Ramadan City. He has published 60 articles in high scientific journals. His research interest fields are "supply chain and logistics modeling", "safety auditing and classification, ergonomics behaviors, waste reduction, TQM, and sustainability viable." He is a Fellow Member of the Engineering Syndicate and Industrial Consultant for Ideal Standard Egypt Company and BestBuy firm. He was awarded the title of Ambassador of Peace (Goodwill) from AFNG 2023.

RAGAB A. EL-SEHIEMY (Senior Member, IEEE) received the B.Sc., M.Sc., and Ph.D. degrees in electrical power systems from Menoufia University, Egypt, in 1996, 2005, and 2008, respectively. He was an Electrical Engineer with Arab Contractor Company for ten years. He joined the Faculty of Engineering, Kafrelsheikh University, Egypt, as an Assistant Researcher, in 2009. He is currently a Full Professor of electrical power systems with Kafrelshiekh University. His research interests include power-system operation, planning, and control, smart grids, renewable energy, and AI and its application to power systems. He is a member of the Electricity and Energy Research Committee, Academy of Research and Technology, Egypt. He was selected as a member of the Arbitration Committee in the Scientific Committee for the Promotion of Professors and Assistant Professors. He was a recipient of the Prof. Mahmoud Khalifia Award in Power System Engineering from the Academy of Research and Technology, in 2016, and the Computer and Information in Industry Award from the Academy of Research and Technology, in 2021. In 2021, he was among the world's top 2% high citations.

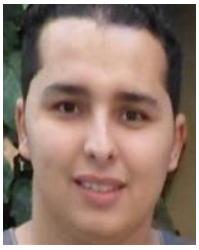

BACHIR BENTOUATI was born in Laghouat, Algeria, in August 1990. He received the License, master's, and Ph.D. degrees in electrotechnical and electrical power systems from the University of Laghouat, in 2010, 2012, and 2018, respectively. His research interests include optimal power flow, artificial intelligence, and optimization techniques.

HASNAA M. EL-ARWASH received the B.S. and M.Sc. degrees in electrical engineering from Menoufia University, Shebin El-Kom, in 1992 and 2006, respectively, and the Ph.D. degree in harmonics mitigation in desalination plants from Tanta University, in 2016. Since 2017, she has been an Assistant Professor with the Mechatronics Department, Alexandria Higher Institute of Engineering and Technology. She has published eight articles in different scientific journals. Her research interests include the development of power quality, solar energy, distribution power systems using artificial intelligence techniques, power system control, particle swarm optimization, linear programming, presentations, optimization methods, global optimization, algorithms, optimization algorithms, multi-objective optimization, optimization modeling, simulation, nonlinear optimization, electrical engineering, swarm intelligence, power systems, genetic algorithm, artificial neural networks, machine learning, and deep learning.